Published in final edited form as:
Biomaterials. 2017 May ; 127: 61–74. doi:10.1016/j.biomaterials.2017.02.035.

Biomaterial-enabled delivery of SDF-1α at the ventral side of breast cancer cells reveals a crosstalk between cell receptors to promote the invasive phenotype

Xi Qiu Liu[a,b,c,d,*], **Laure Fourel**[e,f], **Fabien Dalonneau**[a,b], **Rabia Sadir**[g], **Salome Leal**[a,b], **Hugues Lortat-Jacob**[g], **Marianne Weidenhaupt**[a,b], **Corinne Albiges-Rizo**[e,f], and **Catherine Picart**[a,b,*]

[a]CNRS UMR 5628 (LMGP), 3 parvis Louis Néel, 38016 Grenoble, France

[b]Université Grenoble Alpes, LMGP, 3 parvis Louis Néel, 38016 Grenoble, France

[c]FONDATION ARC, 9 rue Guy Môquet 94803 Villejuif, France

[d]Tongji Medical College, Huazhong University of Science and Technology, Wuhan, 430030, P.R. China

[e]Inserm U1209, Université Grenoble Alpes, Institut Albert Bonniot, Site Santé, 38042 Grenoble cedex 9, France

[f]CNRS UMR5309, Institute for Advanced Biosciences, Institut Albert Bonniot, 38700 La Tronche, France

[g]Institut de Biologie Structurale, UMR 5075, Univ. Grenoble Alpes, CNRS, CEA, F-38027 Grenoble, France

Abstract

The SDF-1α chemokine (CXCL12) is a potent bioactive chemoattractant known to be involved in hematopoietic stem cell homing and cancer progression. The associated SDF-1α /CXCR4 receptor signaling is a hallmark of aggressive tumors, which can metastasize to distant sites such as lymph nodes, lung and bone. Here, we engineered a biomimetic tumoral niche made of a thin and soft polyelectrolyte film that can retain SDF-1α to present it, in a spatially-controlled manner, at the ventral side of the breast cancer cells. Matrix-bound SDF-1α but not soluble SDF-1α induced a striking increase in cell spreading and migration in a serum-containing medium, which was associated with the formation of lamellipodia and filopodia in MDA-MB231 cells and specifically mediated by CXCR4. Other Knockdown and inhibition experiments revealed that CD44, the major hyaluronan receptor, acted in concert, via a spatial coincidence, to drive a specific matrix-bound SDFα-induced cell response associated with ERK signaling. In contrast, the β1 integrin adhesion receptor played only a minor role on cell polarity. The CXCR4/CD44 mediated cellular response to matrix-bound SDF-1α involved the Rac1 RhoGTPase and was sustained solely in the presence of matrix-bound SDFα, in contrast with the transient signaling observed in response to soluble SDF-1α. Our results highlight that a biomimetic tumoral niche enables to reveal potent cellular

Corresponding author. C Picart Tel.: +33 4 56 52 93 11, fax: +33 4 56 52 93 01. catherine.picart@grenoble-inp.fr, xiqiuliu@hust.edu.cn.

Europe PMC Funders Author Manuscripts

effects and so far hidden molecular mechanisms underlying the breast cancer response to chemokines. These results open new insights for the design of future innovative therapies in metastatic cancers, by inhibiting CXCR4-mediated signaling in the tumoral niche via dual targeting of receptors (CXCR4 and CD44) or of associated signaling molecules (CXCR4 and Rac1).

Keywords

Chemokines; SDF-1α/CXCL12; breast cancer cells; metastasis; tumoral niche; hyaluronan; polyelectrolyte multilayer films; CXCR4; CD44

Introduction

Chemokines are small chemoattractant molecules that bind to specific transmembrane receptors at the plasma membrane of target cells [1] and play a central role in the regulation of cell migration, trafficking and metastatic dissemination of cancer cells [2, 3]. SDF-1α (also known as CXCL12) is a major chemokine, which is secreted in bone marrow, lymph nodes, liver and lung [3]. SDF-1α plays a key role in lymphocyte homing, chemotactic response, secretion of angiogenic factors [4] and in a large number of cancers [5]. Its major receptor CXCR4 is expressed at the surface of many types of solid tumors and leukemic cells [5], including malignant breast cancer cells [6]. The cancerous process leads to CXCR4 dysregulation, enhanced signaling and cancer metastasis at distant sites such as lung and bone.

Today, breast cancer is the leading cancer-related death cause among women. In its early stages, breast cancer is usually not fatal but its metastatic spread is responsible for at least 90% of breast cancer-associated mortality [7]. Aggressive breast cancers can metastasize to bone, liver, lung and brain [8] and exhibit an increased CXCR4-signalling [5, 9]. 70% of advanced breast cancer patients, namely HER2 and triple negative patients [9], have skeletal metastasis often leading to mortality [10, 11]. CXCR4 was found to be a prognostic marker of these aggressive breast cancers [5, 9, 12].

Importantly, in the complex ECM microenvironment, cells encounter a multitude of coordinated stimuli that are biochemical, structural and mechanical in nature [13] and the ECM plays a crucial role in the presentation of bioactive molecules [14]. For instance, SDF-1α can interact with ECM components such as heparan sulfates [15], which are important for an appropriate tissue revascularization after induced acute ischemia [16]. SDF-1α can also interact with hyaluronan [17], a structural component in the tumor ECM [18, 19] known to promote tumor progression [20]. By modulating of its interaction with extracellular matrix (ECM) components, SDF-1α is suspected to increase the survival rate of cancer cells in bone marrow [21]. Thus, presentation of chemokines by an appropriate ECM is physiologically relevant both in healthy and cancerous situations [15, 22]. ECM mechanics is another important factor in cell differentiation [23, 24], migration [25, 26], tumor formation and progression [27–31]. High-grade infiltrating ductal carcinoma has a stiffness of ~ 40 kPa [32] and metastasis in the spinal cord of 200-600 kPa [33, 34].

Europe PMC Funders Author Manuscripts

So far the majority of *in vitro* studies, targeting the role of SDF-1α on cancerous processes have been performed by delivering it in solution to cells grown on tissue culture plastic and glass coverslips [35, 36]. These are stiff substrates [37], which are not representative of the microenvironments encountered in tumors. To date, no study aimed at investigating the effects of SDF-1α delivered in a matrix-bound manner on breast cancer adhesion and migration.

Here, we used the layer-by-layer (LbL) technique as a thin biomimetic matrix to deliver SDF-1α to cancer cells in a matrix-bound manner. LbL films allow the precise control of various parameters such as film architecture [38, 39], chemistry, thickness and stiffness [40, 41] to elucidate cell signaling [42]. By carefully selecting the film components and appropriate physico-chemical conditions, it is possible to engineer LbL films that mimic the ECM thin matrix and contain bioactive molecules such as peptides and proteins [43–46]. We recently showed that polyelectrolyte multilayer films made of poly (L-lysine) (PLL) and hyaluronan (HA) can store tunable amounts of the SDF-1α chemokine [45]. In the present study, our aim was to investigate how breast cancer cells respond to SDF-1α delivered locally at their ventral side via such a thin biomaterial. We focused on adhesion and migration, which are two major events of cancer cell metastasis. In contrast to soluble SDF-1α, whose effects were masked in the presence of serum, matrix-bound SDF-1α enabled to reveal, thanks to the spatial proximity of both receptors and to their coincidence signaling, a crosstalk between SDF-1α and the hyaluronan receptor CD44. Both CXCR4 and CD44 drive, in a Rac1-dependent manner, cellular spreading and migration. This spatial coincidence strikingly potentiates the downstream ERK signaling of the ERK1/2 kinase. Our results highlight that a biomaterial presenting SDF-1α in a matrix-bound manner can be used for future cancer therapy studies.

Materials and methods

1 Multilayer film preparation, crosslinking and SDF-1α loading

HA (MW 360,000 g/mol) was purchased from Lifecore (Chaska, MN, USA). PLL (P2636) and PEI (polyethyleneimine, 7×10^4 g/mol) were purchased from Sigma (St-Quentin Fallavier, France). (PLL/HA) film building, crosslinking and SDF-1α loading (Figure 1A) were done as previously described [45]. Briefly, PLL (0.5 mg/mL) and HA (1 mg/mL) were dissolved in Hepes-NaCl buffer (20 mM Hepes at pH 7.4, 0.15 M NaCl). Film deposition on 14 mm glass slides was performed using an automated dipping robot [47]. For 96-well plates, films were manually deposited starting with a first layer of PEI at 5 mg/mL followed by the deposition of a HA-$(PLL/HA)_{12}$ film. Films were crosslinked for 18 h at 4°C using 1-ethyl-3-(3-dimethylamino-propyl) carbodiimide (EDC) at 30 mg/mL and sulfo N-hydrosulfosuccinimide (sulfo-NHS) at 11 mg/mL. Final washing was performed with the Hepes-NaCl buffer for 1 h. The multilayer films will be named hereafter EDC30 film. Such films have a Young's modulus of ~ 200 kPa [41, 48].

Murine SDF-1α was cloned into a pET17b vector, expressed and purified as described previously [45, 49]. For SDF-1α loading into the films, the films were first pre-equilibrated for 30 min in 1 mM HCl. SDF-1α at 100 μg/mL in 1 mM HCl was adsorbed on the films overnight at 4°C. Then, the film-coated glass slides were washed with Hepes-NaCl solution

at regular time intervals during 2 h. The incorporated amount of SDF-1α in the films was measured based on a calibration curve obtained with known amounts of fluorescent SDF-1α in solution as previously reported [45]. The final adsorbed amounts (after thorough rinsing of the films) increased with the initial concentration of SDF-1α in solution (Figure SI1). SDF-1α loaded films were sterilized for 15 min under UV light for downstream cell experiments [45]. SDF-1α delivered in a matrix-bound manner from the films will be named hereafter bSDF. As a control, soluble SDF-1α (1 μg/mL) is added to cells on the polyelectrolyte films and is named hereafter sSDF.

2 Cell culture and antibodies

Human epithelial breast cancer cells (MDA-MB-231) were obtained from ATCC and cultured in DMEM medium supplemented with 10% foetal bovine serum (FBS, PAA Laboratories, Les Mureaux, France) and 1% antibiotics (penicillin G and streptomycin). MCF7 breast adenocarcinoma cell lines (generous gift from L. Lafanechere) were cultured in RPMI supplemented with 10% FCS, insulin (10 μg/mL) and 1% antibiotics (penicillin G and streptomycin). MCF10A cells (generous gift from L. Lafanechere) were culture in RPMI with horse serum (5%) supplemented with epidermal growth factor (25 ng/mL), hydrocortisone (0.5 μg/mL), cholera toxin (1 μg/mL) and insulin (10 μg/mL).

The following antibodies were used for Western Blotting: rabbit-anti-β1 integrin (generous gift from the Albigès-Rizo lab), mouse-anti-CD44 (sc9960, Santa Cruz Biotechnology), rabbit-anti-CXCR4 (ab2074, Abcam), rabbit-anti-phospho-Erk1/2 (#4370, Cell Signaling) and mouse-anti-β tubulin antibody (T4026, Sigma). For immuno-fluorescence, rabbit-anti-CXCR4 (ab2074, Abcam), mouse-anti-β1 integrin (LS-C134368, LifeSpan BioSciences) and rat-anti-CD44 antibodies (553131, clone IM7, BD Pharmingen) were used. For receptor blocking, mouse-anti-β1 integrin blocking antibodies (clone 4B4) were purchased from Beckman Coulter, rat-anti-CD44 (clone IM7) was from BD Pharmingen and mouse-anti-CXCR4 blocking antibodies (clone 12G5) were from R&D Systems. For inhibition studies, the Rac1 inhibitor (NSC23766) was purchased from Calbiochem and the Cdc42 inhibitor (ML141) was from Tocris.

3 Quantification of cell adhesion

MDA-MB231 cells were seeded at 15,000 cells/cm^2 for 16 h. To quantify cell spreading, cells were labeled with rhodamine-phalloidin (1:800, Sigma, France). Fluorescence images were analyzed with ImageJ software (v1.42, NIH, Bethesda) to determine three different parameters: average cell area, circularity and aspect ratio. Cell circularity is defined as $4\pi(A/P^2)$, where A is the cell area and P the perimeter: a circularity value of 1.0 indicates a circular shape, while decreasing values towards 0 indicate an increasingly elongated ellipse. The aspect ratio is defined as the ratio of the length of the Major Axis to the Minor Axis of an ellipse fitted to the cell area. It gives information about the cell elongation.

For the quantification of cell protrusions, the F-actin-dependent cellular protrusions (lamellipodia and filopodia) were determined morphometrically: lamellipodia are highly compact meshworks of actin filaments found at the leading edge of motile cells; filopodia are short bundles of actin filaments, protruding from the cell surface [50].

For inhibition of cell adhesion using anti-integrin antibodies, MDA-MB-231 cells (5×10^4/mL) were pre-incubated for 10 min at RT with different blocking antibodies against β_1 integrin (2 μg/mL), CD44 (1 μg/mL) or CXCR4 (30 μg/mL). Then, the cells were seeded at 15,000 cells/cm^2 on the bSDF films and incubated for 16 h in the presence of the blocking antibodies. For inhibition of signaling proteins, MDA-MB-231 cells were seeded at 15,000 cells/cm^2 on the bSDF films in the presence of Rac1 inhibitor (100 μM) or Cdc42 inhibitor (10 μM), and incubated for 16 h.

4 Cell transfection with small interfering RNAs

SiRNAs against β1 integrin, CD44, CXCR4, Rac 1 and Cdc42 (ON-TARGETplus SMARTpool), silencing respectively human β1 integrin, CD44, CXCR4, Rac1 and Cdc42 were purchased from Thermo Scientific Dharmacon. A scrambled siRNA (All Stars negative control siRNA, Qiagen) was used as a control. For MDA-MB-231 cell transfection with siRNAs, the cells were seeded at 150,000 cells/well in a 6-well plate and cultured overnight. The transfection mix for one well was prepared by adding 6 μL of lipofectamine RNAiMAX Reagent (Invitrogen) to 305 μL of Opti-MEM medium (Gibco) and 0.72 μL of 100 μM siRNA to another 305 μL of Opti-MEM medium. The lipofectamine-containing mix was added to the siRNA-containing mix and incubated for 20 min at room temperature. Prior to transfection the medium in the wells was replaced by medium without antibiotics. Then 610 μL of the final mix were added to each well. After 24 h incubation at 37°C, the cells were transfected for a second time, following the protocol described above and incubated for another 24 h. Then the cells were detached using trypsin-EDTA, seeded at 15,000 cells/cm^2 on the films loaded with SDF-1α and incubated for 16 h.

5 Time-lapse acquisition and quantification of cell migration

For quantification of cell migration on SDF-1α loaded films, MDA-MB-231 cells were seeded at 15,000 cells/cm^2 in different experimental conditions (no SDF, soluble SDF named hereafter sSDF, bSDF). After 4 h at 37°C, cells were imaged every 10 min for 16 h with a 63X oil objective using a LSM 700 confocal microscope (Carl Zeiss Sas, Le Pecq, France) equipped with a controlled environmental chamber (37°C and 5% CO_2). Time-lapse images and movies were assembled using Image J software (v1.42, NIH, Bethesda). Individual cell tracking was performed using the “Manual tracking” plugin, which allows to select a cell, and record its movement by following its position on each frame. At least 20 cells were analyzed for each condition in each independent experiment and two independent experiments were done. All data were analyzed using the “Chemotaxis tool” (Image J), which provides graphic and statistical analysis of the datasets. X/Y calibration and time intervals were fixed based on the parameters of time-lapse images. A summary of all extracted data, including cell migration speeds, was generated under “Statistic feature” of the Image J macro.

6 Immunofluorescence

Cells were fixed with 3.7% formaldehyde for 20 min and permeabilized in 0.2% Triton X-100 for 4 min. For receptor distribution studies, cells were labeled with anti-CXCR4 (1:100), anti-β1 integrin (1:400), or anti-CD44 (1:100) antibodies. Primary antibodies were detected using Alexa Fluor 488-conjugated goat anti-rabbit, Alexa Fluor 568-conjugated

goat anti-mouse, or Alexa Fluor 647-conjugated goat anti-mouse antibodies (at 1:200, Molecular Probes, Invitrogen, France). All the slides were mounted onto coverslips with antifade reagent (Prolong, Invitrogen). Observations were made on an Axiovert 200 M microscope and a LSM 700 confocal microscope (both from Carl Zeiss SAS, Le Pecq, France) using 20X or 63X objectives. Images were acquired with Metaview software using a CoolSNAP EZ CCD camera (both from Ropper Scientific, Evry, France).

7 Gel electrophoresis and immunoblotting

EDC30 films were prepared on 32 mm diameter glass slides with an automated dipping machine (Dipping Robot DR3, Kirstein and Vigler GmbH, Germany) and SDF-1α was loaded at 100 μg/mL. MDA-MB-231 cells were seeded at 15,000 cells/cm^2 on films with or without SDF-1α and incubated for 16 h. In the case of ERK phosphorylation for cells on TCPS, MDA-MB-231 cells were first seeded on TCPS at 15,000 cells/cm^2, then starved in a serum-free medium overnight before being incubated with 1 μg/mL SDF-1α for 0, 5, and 30 min. Cells were then scraped, rinsed in PBS, and lysed in 2×Laemmli sample buffer (Sigma, France). After boiling, 10 μL of total protein samples were loaded and run on 10% polyacrylamide gels before transfer onto PVDF membranes (GE Healthcare, United Kingdom). Membranes were then saturated in 5% BSA in Tris-buffer saline (TBS) that contained 50 mM Tris-HCl and 150 mM NaCl with 0.1% Tween 20 for 1 h and subsequently incubated with antibodies against β1 integrin (1:1000), CD44 (1:100), CXCR4 (1:2000), pERK1/2 (1:2000) and β Tubulin (1:1000). Membranes were washed and incubated with peroxydase-conjugated anti-mouse, anti-rat or anti-rabbit secondary antibodies (Jackson immunoResearch), respectively. Peroxidase activity was visualized by ECL (West pico signal, Pierce) using a ChemiDoc MP imaging system (Bio-Rad).

8 Statistical analysis

Data for at least 50 cells are presented as box plots (1st quartile, median, 3rd quartile, the limits being 10 and 90% and the extreme values 5 and 95%, respectively). Experiments were performed in duplicate or triplicate, with 2 or 3 samples per condition in each experiment. For the quantification of protrusions, vertical bars show the mean % values ± standard deviation for a given cell phenotype, the total number of cells counted for all phenotypes together (L+/F+, L+/F-, L-/F+, L-/F-) being set to 100%. Statistical analysis was performed between more than two groups using analysis of variance (ANOVA) and pair wise comparisons to obtain p values ($p < 0.05$ was considered significant)

Results

1 bSDF increases cell area and cell migration of breast cancer cells

In our previous study, we have shown that controlled and tunable amounts of SDF-1α can be loaded in and released from (PLL/HA) films [45]. Here, we compared two presentation modes of SDF-1α (Figure 1B), with soluble SDF-1α added to cells spread on the polyelectrolyte films (sSDF) or matrix-bound SDF-1α delivered to cells at their ventral side (bSDF). As a negative control, we also studied cells in the absence of SDF-1α (no SDF). Preliminary experiments enabled us to assess that MDA-MB-231 cells responded to bSDF-1α by spreading on soft films in a reproducible manner, when different SDF-1α

batches were used (initial SDF-1α loading concentration 100 μg/mL). In these experimental conditions and after a thorough rinsing of the film, the final bSDF-1α amount was 2.64 ± 0.25 μg/cm^2 as quantified by fluorescence spectroscopy (Figure SI1).

First, we quantified MDA-MB-231 breast cancer cell spreading in different conditions (no SDF, sSDF and bSDF) by staining the actin cytoskeleton (Figure 2). In the absence of SDF or with sSDF, cells were round and poorly spread (Figure 2A) with mean cell areas of 584 ± 169 μm^2 and 689 ± 315 μm^2, respectively (Figure 2B). In contrast, cell spreading on bSDF films was significantly higher with a 3-fold increase in the cell area (1534 ± 543 μm^2). Cell circularity was significantly higher in the absence of SDF and with sSDF (0.84 ± 0.09 and 0.61 ± 0.14, respectively) than with bSDF (0.38 ± 0.13). We verified that UV sterilization did not affect the effect of bSDF on cell attachment and spreading (Figure SI2). In addition, we observed that MDA-MB-231 cells displayed F-actin rich structures at the cell periphery including lamellipodia and filopodia solely in response to bSDF (Figure 2A, arrow). They also appeared elongated and polarized. Due to their heterogenous spreading, we decided to classify the cells according to four different phenotypes (Figure 2C): presenting lamellipodia and filopodia (L+/F+), lamellipodia but no filopodia (L+/F-), no lamellipodia but filopodia (L-/F+), and finally cells devoid of lamellipodia and filopodia (L-/F-). We quantified the % of cells in each category for the three experimental conditions (Figure 2D). In the absence of SDF, 96.2 ± 6.2% of the cells were round without lamellipodia or filopodia. sSDF slightly increased the formation of protrusions, with 7.2 ± 5.2 % presenting the L+/F- and 12.0 ± 10.3 % the L-/F+ phenotypes, respectively. However, there were only a few cells presenting both lamellipodia and filopodia (L+/F+, 2.5 ± 1.4%). In contrast, bSDF promoted the formation of both lamellipodia and filopodia with 37.3 ± 10.2% of the cells being L+/F+. Furthermore, 21.2 ± 13.3 % of the cells exhibited only lamellipodia and 20.3 ± 9.7% only filopodia. In total, there were more than 78% of the cells exhibiting protrusions, whether lamellipodia or filopodia or both, versus 3.8 % and 21.7 % with no SDF or sSDF, respectively (Figure 2D).

Thus, our results show that the formation of protrusions was specifically induced by the presentation of SDF in a matrix-bound manner while soluble SDF only rarely induced protrusions.

The bSDF1-mediated cell response on cell spreading was confirmed on two other breast cancer cell lines, MCF-7 cells, which are reported to be malignant but non-invasive cells and MCF10A cells, which are immortalized by non-malignant [51]. MCF-7 are known to respond to SDF1α since they express its receptors [52, 53]. Similarly to MDA-MB231 cells, we found that MCF-7 barely adhered and were very round on the EDC30 films (Figure SI3). They remain so, even in the presence of sSDF-1α . In contrast, they were more spread on bSDF-1 and exhibited numerous protrusions (Figure SI3). There was a 53 % increase in cell spreading (565 ± 186 μm^2 with no SDF versus 865 ± 273 μm^2 with bSDF) associated with a loss of circularity (0.65 ± 0,18 with on SDF versus 0.44 ± 0,12 with bSDF). bSDF promoted the formation of lamellipodia with 37.0 ± 22.9 7% of the cells being (L+/F-) in comparison to 3.5 ± for 3.5 for no SDF. MCF10A cells also responded to bSDF (Figure SI4) with a drastic increase in cell spreading (2.9 fold from 449 ± 175 μm^2 with no SDF to 1317 + 358 μm^2 with bSDF) and decrease in circularity index (0.77 ± 0.12 with no SDF versus 0.52

± 0,18 with bSDF). However, this cell spreading was not associated with lamellipodia or filopodia formation (Figure SI4). These data clearly show that, in addition to MDA-MB231 cells, MCF7 and MCF10A cells respond to matrix-bound SDF in a different manner, by an increased spreading and by become protrusive in the case of MCF7 cells.

Soluble SDF-1α is already known to trigger breast cancer cell migration in chemotaxis assays using porous membranes ("Transwells"), when there is no added serum in the culture medium [36, 54]. We next addressed the question whether bSDF and sSDF could influence the migration of the most invasive cells, the MDA-MB-231 cells [55], in our culture conditions (serum-containing growth medium). Time-lapse experiments were performed for cells cultured on the different films for 16 h (Figure 3). Representative migration tracks of cells are shown in Figure 3A as well as the quantification of the cell migration speed (Figure 3B). In the absence of SDF-1α, MDA-MB-231 cells migrated randomly on films at 21.0 ± 8.4 μm/h. sSDF slightly but non significantly increased the cell migration speed to 26.4 ± 8.0 μm/h, while bSDF significantly increased cell migration to 57.0 ± 17.4 μm/h ($p < 0.05$). Note that we did not observe a directional migration, which may be due to the homogeneous presentation of SDF-1α in the films.

Together, our data show that there is an increase of spreading, of protrusions and of migration of MDA-MB-231 breast cancer cells in response to SDF presented by LbL films.

2 Breast cancer cell response to bSDF involves both CXCR4 and CD44 receptors

We next investigated whether the adhesive and migratory response of MDA-MB-231 cells upon SDF presentation might involve adhesion receptors, in addition to the SDF-1α receptor (Figure 4). CXCR4 is known to be the major SDF-1α receptor in MDA-MB-231 cells [56]. Besides, these cells are known to express one of the adhesive receptors, CD44 known to interact with hyaluronan which is the polyanionic component of the LbL film and an important component in the tumor-associated stromal ECM [57]. MDA-MB-231 cells also express high levels of the β1 integrin adhesion receptor [58, 59], which is involved in cell-ECM interactions or adhesive structures [56–58], in comparison to other beta chain integrins such as β3, which are also known to be involved in metastasis [59].

We observed the spatial distribution of CXCR4, CD44 and β1 integrins in bSDF-spread cells by confocal microscopy (Figure 4A). Whereas CXCR4 exhibited a homogeneous and punctuate distribution all over the cell, both CD44 and β1 integrin are concentrated together in adhesive patches localized at the edge of cellular protrusions in focal adhesions. Furthermore, filopodia were positive for CD44 but devoid of CXCR4 at their tips.

Quantitative expression of the three receptors was assessed by Western blot in the absence or presence of bSDF (Figure 4B). The Western blots confirmed that CXCR4, CD44 and β1 integrins are expressed in MDA-MB-231 cells plated on the films in the absence of SDF. bSDF induced a slight increase in both CXCR4 and CD44 without significant difference as judged from the quantification of signals obtained using Western blots (Figure 4C). The expression level of β1 integrin was not changed. Our results indicate that, beside the CXCR4 chemokine receptor, an adhesion receptor, CD44, may come into play in the MDA-MB-231 cell response to bSDF.

In order to investigate the respective roles of CXCR4, CD44 and β1 integrin in the cell response induced by bSDF, we knocked down the expression of these receptors (Figure 5) to analyze their impact on cell spreading area and cell circularity (Figure 5A and B), aspect ratio (Figure 5C) and the formation of protrusions (Figure 5D). The efficiency of siRNA-mediated receptor silencing was confirmed by Western blotting (Figure 5E). Both CXCR4 and CD44 inhibition using blocking antibodies (Figure SI5) or siRNA silencing (Figure 5 A,B) led to a significant decrease in cell area to 50.3 ± 10.1% and 47.6 ± 10.9%, respectively, compared to cells on bSDF with a control siRNA, which was associated with an increase in their circularity. Qualitatively similar differences were obtained with a significant loss of cell spreading, aspect ratio and increase in circularity when CXCR4 or CD44 are blocked. In contrast, β1 integrin silencing (Figure 5B) or blocking (Figure SI5) did not significantly affect cell area nor circularity, and the aspect ratio slightly decreased but was still high (Figure 5B), showing that cells retained part of their polarity.

Importantly, MDA-MB-231 cells lost the majority of their protrusions and mostly became devoid of lamellipodia in response to CXCR4 and CD44 silencing (Figure 5D). The proportion of L+/F+ cells dropped from 37.3 ± 10.2% (siControl) to 19.7 ± 13.4% and 5.5 ± 3.7%, for siCXCR4 and siCD44, respectively. The proportion of L+/F- cells, which was 21.2 ± 13.4% for the siControl, dropped to 4.8 ± 1.2% and 0.6 ± 1.2%, respectively for siCXCR4 and siCD44. Thus, the effect of CD44 silencing on lamellipodia formation was stronger than that induced by CXCR4 silencing. β1 integrin silencing, surprisingly, also led to an increase in the proportion of L+/F+ cells from 37.3 ± 10.2% to 69.4 ± 6.0% in comparison to the control, while the proportion of L-/F- cells decreased from 21.1 ± 5.5% to 1.1 ± 1.5%.

To investigate possible functions of β1 integrin on cell adhesion and spreading on the polyelectrolyte films, we also performed experiments on stiffer films (EDC70). In contrast to EDC30 films, MDA-MB -231 cells were able to spread on EDC70 in the absence of SDF-1α (Figure SI6) On such stiffer films, cell area and protrusions (especially lamellipodia) significantly decreased after β1 integrin blocking (Figure SI6A) and silencing (Figure SI6B), showing a role of β1 in stiffness sensing.

Next, time lapse microscopy was used to determine the effects of CXCR4, CD44 and β1 integrin on bSDF-induced cell migration (Figure 6). The cell tracks are shown in Figure 6A. Cell migration speed significantly decreased from 65.1 ± 14.0 μm/h (siControl) to 30.8 ± 11.3 μm/h and 26.7 ± 10.7 μm/h after silencing CXCR4 and CD44, respectively (Figure 6B). In contrast, knocking-down β1 integrin slightly but non-significantly decreased the cell migration speed to 51.1 ± 15.0 μm/h.

Altogether, our results demonstrate that, beside the SDF-1α receptor CXCR4, the adhesion receptor CD44 is a key actor in MDA-MB-231 cell adhesion and migration in response to bSDF, while the adhesion receptor β1 integrin rather plays a role in cell polarization.

4 bSDF induces ERK1/2 phosphorylation in a Rac1-dependent manner

Rac1 and Cdc42 are two members of the Rho GTPase family involved in actin reorganization [50]. Rac1 is essential for lamellipodial protrusions while Cdc42 triggers the

formation of filopodia [50, 60, 61]. To investigate a potential link between bSDF-induced cellular effects and Rac1 or Cdc42 signaling, we analyzed cell spreading, circularity and protrusion formation after inhibition of Rac1 or Cdc42 signaling using either inhibitors or siRNA-mediated silencing (Figure 7). Rac1 inhibition using NSC23766 strongly decreased bSDF-induced cell spreading, while the Cdc42 inhibitor (ML141) had no significant effect (Figure 7A,B). In addition, the proportions of L+/F+ cells decreased from 52.4 ± 15.2% to 3.7 ± 0.9% and 9.3 ± 8.6%, respectively in the presence of Rac1 and Cdc42 inhibitors (Figure 7C). 77.0 ± 1.8% of the cells were without protrusion (L-/F-) in the presence of Rac1 inhibitor, in comparison to 15.7 ± 7.3% for bSDF, while 79.4 ± 6.3% of the cells exhibited lamellipodia but no more filopodia (L+/F-) in the presence of the Cdc42 inhibitor compared to 14.4 ± 9.1% for the control (Figure 7C).

Besides, we noted a decrease of the L-/F+ population from 14.4 ± 9.1% (control) to 4.2 ± 3.2% after Cdc42 inhibition, while there was no change for the Rac1 inhibitor with respect to this phenotype (17.2 ± 5.8%). This highlighted, as anticipated, that filopodia formation was Cdc42-dependent and not Rac1-dependent (Figure 7).

Silencing Rac1 and Cdc42 activity, using siRNA mediated knock-down, qualitatively confirmed these results (Figure 7D,E,F). In the case of Rac1 silencing, there was a statistically significant decrease in cell area (to 39.3 ± 13.6% of the control) and an increase in cell circularity (0.52 ± 0.15 in comparison to 0.28 ± 0.07 for the control) (Figure 7E). In addition there was a drastic increase in the number of cells presenting an L-/F- phenotype, with 65.4 ± 14.9% in comparison to 14.2 ± 9.23% for the control (Figure 7F). In contrast, silencing Cdc42 strongly decreased the proportion of cells that exhibited filopodia (6.0 + 5.0% versus 20.0 + 10.3% for the siControl), but that of lamellipodia L+/F- was similar (63.0 ± 6.2%versus 60.5 + 10.7 for the siControl).

It is known that signal transduction of soluble SDF-1α via CXCR4 involves a major pathway, the mitogen-activated protein kinase (MAPK) pathway, which leads to ERK1/2 phosphorylation, important for chemotaxis [62, 63] [64]. Therefore, we next determined the effects of bSDF on the activation of ERK1/2 in MDA-MB-231 cells in comparison to its soluble presentation (Figure 8). In the case of sSDF-1α added at 1 μg/mL to serum-starved cells grown on tissue culture polystyrene (TCPS), ERK1/2 phosphorylation was observed 5 min after addition of the chemokine but quickly returned to its basal level after 30 min (Figure 8A). Interestingly, bSDF induced a sustained signaling of phospho-ERK in MDA-MB231 cells after 16 h, but not in the control group of cells incubated without SDF1α (No SDF) or with soluble (sSDF) (Figure 8B). CXCR4 and, to a greater extent CD44 silencing greatly decreased bSDF-induced ERK1/2 phosphorylation (Figure 8C), with a 60% loss of signaling after CD44 silencing (Figure 8D). Furthermore, Rac1 silencing also drastically decreased ERK phosphorylation in comparison to Cdc42 silencing (Fig. 8E and F).

Together, these results demonstrate that bSDF triggers the phosphorylation of ERK under the control of CD44 and Rac1.

Discussion

bSDF-1α is sufficient to trigger MDA-MB231 cell adhesion, migration and the formation of protrusions

SDF-1α is an important chemokine playing a key role in hematopoietic stem cell homing [65], development and cancer metastasis [66, 67]. It interacts mostly with the CXCR4 receptor, which is expressed by MDA-MB-231 breast cancer cells and other breast cancer cell lines (Figure 4 and [36]{Salazar, 2014 #177}). Indeed, recent meta-analysis studies have shown that an increased expression of CXCR4 during the progression of breast cancer cells is an indicator of poor prognosis [68, 69]. It is already known using soluble SDF-1α that SDF-1α/CXCR4 signaling has an important role in cell cytoskeleton rearrangement, protrusion formation and migration [36]. Furthermore, both SDF-1α and CXCR4 can act in concert to increase the aggressiveness of breast cancer [70].

Using the layer-by-layer film as a tunable platform, we show that SDF-1α presented by the matrix, and not as a soluble cue, is able to induce breast cancer cell spreading, migration and protrusion formation. The EDC30 films (E ~ 200 kPa) [48] have a stiffness close to the metastasis matrix in the spinal cord [33]. The matrix-bound presentation of SDF-1α by the films to CXCR4-expressing breast cancer cells can thus mimic a tumoral niche.

To our knowledge, we showed here for the first time that a matrix-bound chemokine can trigger breast cancer cell adhesion of three different cell lines, MCF10A, MCF7 and MDA-MB231. Our data are reminiscent of the bSDF-induced spreading of myoblast cells on low crosslinked polyelectrolyte films [45] and of T-lymphocyte cells on glycosaminoglycan-biomimetic platforms [71].

The bSDF-induced cellular protrusive activity was characterized in by the presence of lamellipodia in MCF7 cells (Figure S3) and lamellipodia and filopodia in MDA-MB231 cells (Figure 2) These protrusions are reminiscent of the protrusions induced in CD34+ human progenitor cells plated on a hyaluronan-coated surface, when these cells were exposed to soluble SDF-1α [72]. bSDF was able to drastically increase cell migration in a serum-containing growth medium (Figure 3), where the effects of soluble SDF-1α were masked. This highlights that the local concentration of bSDF at the ventral side of the cell was sufficient to trigger cell migration. Our data with bSDF are in agreement with previous chemotaxis (Transwells) assays using sSDF in a low serum-containing medium, which was necessary to unveil the specific effects of the soluble chemokine [36, 54].

A direct comparison between soluble and matrix-bound concentrations of SDF-1α locally at the cellular membrane is difficult, as bSDF targets the ventral side of the cells whereas sSDF can target any available receptor but mostly those at the dorsal side of the cell. The matrix-bound presentation enables to increase the local concentration of the chemokine at the cell membrane in view of the reduced dimensionality [73]: 2D surface presentation for bSDF in comparison to 3D for the freely diffusing sSDF molecule. One can get a rough estimate of the number of CXCR4 receptors knowing that there are ~163,521 ± 35,875 binding sites/cell for SDF-1α in Jurkat cells [74], which are a positive control for CXCR4 expression. This would correspond to ~ 230 binding sites/μm^2 of cell surface area, considering a Jurkat cell

area of 700 μm^2. The bSDF concentration used here (2.6 μg/cm^2) would thus correspond to ~2x10^6 SDF-1α molecules/μm^{2}of film. This should theoretically be enough to saturate the endogenous SDF-1α receptors in MDA-MB-231 cells.

Beta1 integrin is not involved in bSDF-induced cell response on soft films but rather in stiffness sensing on stiff films

The integrin family of surface receptors also play a critical role in many cellular processes that include cell adhesion, cell spreading, growth signaling [75, 76], as well as mediating cell migration towards soluble stimulants/growth factors. Integrins are known to be mechano-sensors that transduce stiffness-sensing from the ECM into biochemical events and stimulate cytoskeletal remodeling [77, 78]. Indeed, the tumor stroma is characterized by ECM remodeling and stiffening [78]. β1 integrin, which is the most expressed integrin in MDA-MB231 cells [59] was chosen as a candidate to study its functions in bSDF-induced cell behavior. We found that its spatial distribution at the tips of protrusions was similar to that of CD44 on well-spread cells on bSDF films and that was localized in focal adhesions (Figure 4A). Since the polyelectrolyte film itself is not presenting an integrin ligand, β1 integrin may bind to fibronectin coming from the serum or secreted by the cells.

Notably, bSDF did not stimulate the expression of β1 integrin, in contrast to that of CD44 (Figure 4B, C). Besides, after silencing of β1 integrin using siRNA, bSDF-induced cell spreading and migration on soft films was only slightly but not significantly impaired whereas cell polarity, as characterized by the aspect ratio, was affected (Figure 5 and 6). Indeed, β1 integrin was rather a negative regulator of the protrusion formation as the proportion of L+/F+ cells drastically increased after β1 silencing (Figure 5).

MDA-MB-231 cells spread well and form protrusions on stiffer films (EDC70) without SDF-1α (Figure SI6), which is consistent with previous results obtained for other cancer cells on collagen gels of increasing stiffness [27]. On the stiff films, we found that cell spreading and protrusion formation was significantly impaired after β1 integrin blocking (Figure SI6A) or silencing (Figure SI6B), showing a role of β1 integrin in stiffness sensing of polyelectrolyte films. Altogether, our results indicate that β1 integrin has a minor role in the bSDF-induced cell spreading, protrusion formation and migration on soft polyelectrolyte films but is rather involved in stiffness sensing.

CD44 involvement in the CXCR4-mediated cell response in a Rac1-dependent manner is also related to ERK signaling

Our results show that bSDF-induced MDA-MB-231 cancer cell spreading, migration, and protrusion formation strongly depend on the HA adhesion receptor CD44 (Figure 5, 6), as CD44 blocking or silencing drastically reduced cell spreading, migration and completely changed the cell phenotype to round cells devoid of lamellipodia and filopodia, and impaired ERK signaling. CD44 was localized at the tips of protrusions in filopodia devoid of CXCR4 (Figure 4). In addition, bSDF-induced CD44 expression in MDA-MB-231 cells (Figure 2).

CD44 is already known to be an important adhesion receptor in breast cancer progression [79] but its dual role as tumor promotor or suppressor has been highly debated [80]. However, recent studies on cancer stem cell markers suggest that its expression may depend

Europe PMC Funders Author Manuscripts

on the breast cancer subtype [80], with a low expression for luminal cancers and a high overexpression for basal breast cancers [81].

Interestingly, our results using bSDF are consistent with short-term actin cytoskeleton changes already observed in other cell types, especially in hematopoietic progenitor cells that were plated on HA-coated surfaces in the presence of soluble SDF-1α [72]. For these cells, the CD44-positive protrusions were also devoid of CXCR4. This initial study [72] using soluble SDF-1α clearly suggested a crosstalk between the CD44 and CXCR4 receptors although the authors did not study the effect of receptor silencing. Our data are also in agreement with the uropod formation of human promyelocytic leukemia cells [82] observed in response to soluble SDF-1α when cells were plated on HA-coated substrates in vitro. Interestingly, co-presentation of HA and SDF-1α using engineered HA hydrogels was found to stimulate bone marrow derived cell chemotaxis [17], also suggesting that CD44 and CXCR4 may act in synergy.

Thus, the crosstalk between the SDF-1α receptor CXCR4 and the HA receptor CD44 may be a common feature of different cell types and ECM contexts, in which cell adhesion to the extracellular matrix and migration are important, provided that both receptors can interact with their ligands in close proximity. This crosstalk may either be induced by bSDF as we showed here via our bSDF-1α-presenting biofilm, or by surface coatings of HA in combination with sSDF as shown in previous studies [72, 82].

We further showed here that Rac 1 is involved in the bSDF-induced formation of protrusions (Figure 7) in MDA-MB231 cells, and that both CD44 and Rac1 act in concert in the bSDF-1α-induced ERK phosphorylation (Figure 8). Our data are in agreement with the identified role of CD44 in the migration of a hepatoma cell line in the presence of HA [83] as well as on its identified role in ERK phosphorylation. However, ERK phosphorylation induced by sSDF is known to be a short-term and time-dependent process [62, 63, 84], with phosphorylation usually lasting for no longer than 30 min. Our data clearly showed that only bSDF induced a sustained ERK phosphorylation up to at least 16 h of adhesion (Figure 8). This highlights that the effect of the chemokine presented in a matrix-bound manner at the ventral side of the cells is much more potent than its transient and short-term signaling when added in solution. This is especially important in view of the fact that sustained ERK signaling is known to have important consequences in the control of the proliferative cyclin D1 activity and in this way could guide cell proliferation or differentiation [85, 86]. It is likely that the bSDF-induced sustained ERK signaling is an early hallmark of cell fate change, which will lead in the longer term to a phenotypic switch of MDA-MB231 cells.

The major differences between bSDF and sSDF presentations and downstream signaling are summarized in Figure 9. sSDF mostly interacts with its receptor CXCR4 at the dorsal side of the cancer cells (Figure 9A), thus the cells are round with few filopodia (Figure 2) and signaling of pERK after Rac 1 activation is only transient (Figure 8). The intensity of the pERK signal is low and transient. In this context, the HA receptor CD44 is unlikely to cooperate with CXCR4 since HA is solely provided by the pericellular coat. In contrast, bSDF mostly interacts with its receptor CXCR4 at the ventral side of the cancer cells (Figure 9B), where there is a very high local concentration of SDF-1α molecules provided by the

biomimetic film (Figure 9). This interaction leads to a clustering of CXCR4 receptors at the cell membrane. In this particular spatial configuration, CD44 receptors are also clustering due to the proximity of HA in the pericellular coat and the biomimetic polyelectrolyte film and the cells exhibit a very high protrusive activity (Figure 2) and are highly motile (Figure 3). In view of their spatial proximity, both receptors (CXCR4 and CD44) will cooperate leading to an enhanced Rac1-mediated cell protrusive activity (Figure 5 and Figure 7). In terms of signaling, this crosstalk increases the amount of pERK (higher signal intensity) as well as the duration of the signal (sustained signaling) (Figure 8). Although we do not know whether, in breast cancer cells, this cooperation occurs via a direct receptor interaction at the cell membrane or via an internal biochemical signaling mechanism triggered between CXCR4 and CD44, recent data obtained in endothelial cells and hepatocytes by Fuchs et al. [83] showed, using co-immunoprecipitation, that there is a direct physical interaction between CXCR4 and CD44. This interaction was revealed in the presence of soluble SDF-1α , which was the only presentation mode they studied [83]. We hypothesize that a two-step mechanism is occurring in the potent bSDF-induced ERK signaling: first, MDA-MB-231 breast cancer cells interact with bSDF-1α via CXCR4, which activates the latter. Second, CD44 can be activated and bind to its ligand HA, which is present in the breast cancer pericellular coat [57] and in the polyelectrolyte film. In our settings, it is clearly the spatial proximity of the ligands SDF-1α and HA in the biomimetic niche and of their respective receptors (CXCR4 and CD44) at the cellular membrane that is key to facilitate their crosstalk, induce protrusive activity and amplify pERK signaling.

The crosstalk between CXCR4 and CD44 in the context of breast cancer cells is particularly relevant, since aggressive tumors of HER2 patients (one of the category of aggressive cancers based on histopathological analysis commonly used in clinical practice) respond to inhibitors of CXCR4 [9]. Thus, our present findings may help to develop innovative cancer therapies by improving the specificity of the treatment against CXCR4-signaling. For instance, CXCR4 and CD44 receptors may be selectively and simultaneously inhibited via a dual therapy, or inhibitors of CXCR4 may be combined with an inhibitor of hyaluronan synthase in order to decrease CD44 signaling. Alternately, both CXCR4 and Rac1 may be targeted in a dual therapy, as was recently suggested as new therapeutic route [87]. In the future, it will be interesting to further explore and understand the different behaviors of MCF10A, MCF7 and MDA-MB231 cells, which are representative of different types of cancers. Their different malignancy and invasiveness may be characterized by distinct molecular responses on bSDF films.

The crosstalk we evidenced here *in vitro* in the context of MDA-MB231 breast cancer cells and matrix-bound SDF-1α can have an *in vivo* relevance in different cellular niches. Indeed, it likely explains why delivery of SDF-1α via HA hydrogels enhances bone marrow cell homing to the remodeling myocardium after cardiac injury [17], since bone marrow cells also express CD44 receptors [72].

Knowing the crucial role of SDF-1α in cell homing, the bSDF-presenting films studied here in the context of breast cancer adhesion and migration may be more broadly applied to other cell types, such as tumor cells of different grades and with different levels of CXCR4 expression [36], or hematopoietic cells, in order to further decipher the potent molecular

Europe PMC Funders Author Manuscripts

events driven the matrix-bound presentation of chemokines in specific cell niches. Since our biomaterial is a versatile platform that can present other growth factors, such as bone morphogenetic proteins [73], or bioactive peptides [46], our proof-of concept study revealing a biomaterial-driven spatial coincidence of receptors, namely CXCR4 and CD44, opens new avenues not only for regenerative medicine but also for studies of other cancers and future developments of innovative therapies via high throughput screening of anti-cancerous drugs.

Conclusions

In this study, we used biopolymeric thin films as a biomimetic tumoral niche to present the SDF-1α chemokine in a matrix-bound manner to breast cancer cells. Matrix-bound SDF-1α notably increased cell spreading and migration, via the formation of protrusions, especially lamellipodia and filopodia while soluble SDF-1α had little effect. We evidenced that the SDF-1α receptor CXCR4 acts in concert with the adhesion receptor CD44 in the cell response to matrix-bound SDF-1α The binding of the CD44 receptor to its ligand HA is possible since HA is present both in the pericellular coat of the cancer cells and in the biomimetic film. The spatial coincidence of CXCR4/CD44 receptor cooperation specifically involved the RhoGTPase Rac1. In comparison to CD44, β1 integrin played a less important role in the soft tumoral niche but still influenced cell polarization as proved by the change in aspect ratio. A major SDF-1α signaling pathway characterized by ERK phosphorylation in a Rac-1 dependent manner was specifically activated and strongly potentiated in response to matrix-bound SDF-1α via the spatial coincidence with CD44. Thus, our study may help to design future regenerative therapies against breast cancer cells: a specific inhibition of CXCR4 signaling to decrease ERK phosphorylation can be improved by dual therapy against CXCR4 and CD44-signaling, or against CXCR4 and Rac1 signaling. More broadly, our work open new perspectives for the use of biomimetic tumor niches in cancer and hematopoietic cell research, providing a biologically relevant presentation mode of the chemokines.

Supplementary Material

Refer to Web version on PubMed Central for supplementary material.

Acknowledgements

This research was supported by the "Association Recherche contre le Cancer" via a post-doctoral fellowship to XQL (ARC, PDF20121206052) and the Agence Nationale de la Recherche (ANR-NT05-4-41968-Chemoglycan). This work was supported by the European Commission in the frame of FP7 (ERC Starting Grant BIOMIM, GA 239370 to CP), by the FRM (CAR) and by the Ligue Nationale contre le Cancer for Equipe labellisée Ligue 2014 (CAR). CP is a senior member of Institute Universitaire de France, whose support is acknowledged. The groups of C.P. and C.A.R. belong to the CNRS consortium CellTiss. We thank Thomas Boudou, Franz Bruckert and Matt Kutys for fruitful discussions and technical advices. We are also grateful to Laurence Lafanechere and Sophie Michallet for providing the MCF-7 cells and advices on cell culture.

Bibliographic references

[1]. Murphy PM. Chemokines and the molecular basis of cancer metastasis. N Engl J Med. 2001; 345:833–5. [PubMed: 11556308]

[2]. Homey B, Muller A, Zlotnik A. Chemokines: agents for the immunotherapy of cancer? Nat Rev Immunol. 2002; 2:175–84. [PubMed: 11913068]

[3]. Kucia M, Jankowski K, Reca R, Wysoczynski M, Bandura L, Allendorf DJ, Zhang J, Ratajczak J, Ratajczak MZ. CXCR4-SDF-1 signalling, locomotion, chemotaxis and adhesion. J Mol Histol. 2004; 35:233–45. [PubMed: 15339043]

[4]. Janowska-Wieczorek A, Marquez LA, Dobrowsky A, Ratajczak MZ, Cabuhat ML. Differential MMP and TIMP production by human marrow and peripheral blood CD34(+) cells in response to chemokines. Exp Hematol. 2000; 28:1274–85. [PubMed: 11063876]

[5]. Furusato B, Mohamed A, Uhlen M, Rhim JS. CXCR4 and cancer. Pathol Int. 2010; 60:497–505. [PubMed: 20594270]

[6]. Smith MC, Luker KE, Garbow JR, Prior JL, Jackson E, Piwnica-Worms D, Luker GD. CXCR4 regulates growth of both primary and metastatic breast cancer. Cancer Res. 2004; 64:8604–12. [PubMed: 15574767]

[7]. Mehlen P, Puisieux A. Metastasis: a question of life or death. Nat Rev Cancer. 2006; 6:449–58. [PubMed: 16723991]

[8]. Chambers AF, Groom AC, MacDonald IC. Dissemination and growth of cancer cells in metastatic sites. Nat Rev Cancer. 2002; 2:563–72. [PubMed: 12154349]

[9]. Lefort S, Thuleau A, Kieffer Y, Sirven P, Bieche I, Marangoni E, Vincent-Salomon A, Mechta-Grigoriou F. CXCR4 inhibitors could benefit to HER2 but not to triple-negative breast cancer patients. Oncogene. 2016

[10]. Bussard KM, Gay CV, Mastro AM. The bone microenvironment in metastasis; what is special about bone? Cancer Metastasis Rev. 2008; 27:41–55. [PubMed: 18071636]

[11]. Coleman RE. Skeletal complications of malignancy. Cancer. 1997; 80:1588–94. [PubMed: 9362426]

[12]. Ablett MP, O'Brien CS, Sims AH, Farnie G, Clarke RB. A differential role for CXCR4 in the regulation of normal versus malignant breast stem cell activity. Oncotarget. 2014; 5:599–612. [PubMed: 24583601]

[13]. Provenzano PP, Keely PJ. Mechanical signaling through the cytoskeleton regulates cell proliferation by coordinated focal adhesion and Rho GTPase signaling. J Cell Sci. 2011; 124:1195–205. [PubMed: 21444750]

[14]. Hynes RO. The extracellular matrix: not just pretty fibrils. Science. 2009; 326:1216–9. [PubMed: 19965464]

[15]. Lortat-Jacob H. The molecular basis and functional implications of chemokine interactions with heparan sulphate. Curr Opin Struct Biol. 2009; 19:543–8. [PubMed: 19800217]

[16]. Rueda P, Richart A, Recalde A, Gasse P, Vilar J, Guerin C, Lortat-Jacob H, Vieira P, Baleux F, Chretien F, Arenzana-Seisdedos F, et al. Homeostatic and tissue reparation defaults in mice carrying selective genetic invalidation of CXCL12/proteoglycan interactions. Circulation. 2012; 126:1882–95. [PubMed: 23035208]

[17]. Purcell BP, Elser JA, Mu A, Margulies KB, Burdick JA. Synergistic effects of SDF-1alpha chemokine and hyaluronic acid release from degradable hydrogels on directing bone marrow derived cell homing to the myocardium. Biomaterials. 2012; 33:7849–57. [PubMed: 22835643]

[18]. Lokeshwar VB, Rubinowicz D, Schroeder GL, Forgacs E, Minna JD, Block NL, Nadji M, Lokeshwar BL. Stromal and epithelial expression of tumor markers hyaluronic acid and HYAL1 hyaluronidase in prostate cancer. J Biol Chem. 2001; 276:11922–32. [PubMed: 11278412]

[19]. Lokeshwar VB, Cerwinka WH, Isoyama T, Lokeshwar BL. HYAL1 hyaluronidase in prostate cancer: a tumor promoter and suppressor. Cancer Res. 2005; 65:7782–9. [PubMed: 16140946]

[20]. Xu X, Gurski LA, Zhang C, Harrington DA, Farach-Carson MC, Jia X. Recreating the tumor microenvironment in a bilayer, hyaluronic acid hydrogel construct for the growth of prostate cancer spheroids. Biomaterials. 2012; 33:9049–60. [PubMed: 22999468]

[21]. Sison EA, Brown P. The bone marrow microenvironment and leukemia: biology and therapeutic targeting. Expert Rev Hematol. 2011; 4:271–83. [PubMed: 21668393]

[22]. Monneau Y, Arenzana-Seisdedos F, Lortat-Jacob H. The sweet spot: how GAGs help chemokines guide migrating cells. J Leukoc Biol. 2016; 99:935–53. [PubMed: 26701132]

[23]. Engler AJ, Carag-Krieger C, Johnson CP, Raab M, Tang HY, Speicher DW, Sanger JW, Sanger JM, Discher DE. Embryonic cardiomyocytes beat best on a matrix with heart-like elasticity: scar-like rigidity inhibits beating. J Cell Sci. 2008; 121:3794–802. [PubMed: 18957515]

[24]. Engler AJ, Sen S, Sweeney HL, Discher DE. Matrix elasticity directs stem cell lineage specification. Cell. 2006; 126:677–89. [PubMed: 16923388]

[25]. Hadjipanayi E, Mudera V, Brown RA. Guiding cell migration in 3D: a collagen matrix with graded directional stiffness. Cell Motil Cytoskeleton. 2009; 66:121–8. [PubMed: 19170223]

[26]. Lo CM, Wang HB, Dembo M, Wang YL. Cell movement is guided by the rigidity of the substrate. Biophys J. 2000; 79:144–52. [PubMed: 10866943]

[27]. Paszek MJ, Zahir N, Johnson KR, Lakins JN, Rozenberg GI, Gefen A, Reinhart-King CA, Margulies SS, Dembo M, Boettiger D, Hammer DA, et al. Tensional homeostasis and the malignant phenotype. Cancer Cell. 2005; 8:241–54. [PubMed: 16169468]

[28]. Provenzano PP, Inman DR, Eliceiri KW, Keely PJ. Matrix density-induced mechanoregulation of breast cell phenotype, signaling and gene expression through a FAK-ERK linkage. Oncogene. 2009; 28:4326–43. [PubMed: 19826415]

[29]. Ulrich TA, de Juan Pardo EM, Kumar S. The mechanical rigidity of the extracellular matrix regulates the structure, motility, and proliferation of glioma cells. Cancer Res. 2009; 69:4167–74. [PubMed: 19435897]

[30]. Wozniak MA, Desai R, Solski PA, Der CJ, Keely PJ. ROCK-generated contractility regulates breast epithelial cell differentiation in response to the physical properties of a three-dimensional collagen matrix. J Cell Biol. 2003; 163:583–95. [PubMed: 14610060]

[31]. Pickup MW, Mouw JK, Weaver VM. The extracellular matrix modulates the hallmarks of cancer. EMBO reports. 2014; 15:1243–53. [PubMed: 25381661]

[32]. Samani A, Zubovits J, Plewes D. Elastic moduli of normal and pathological human breast tissues: an inversion-technique-based investigation of 169 samples. Phys Med Biol. 2007; 52:1565–76. [PubMed: 17327649]

[33]. Dalton PD, Flynn L, Shoichet MS. Manufacture of poly(2-hydroxyethyl methacrylate-co-methyl methacrylate) hydrogel tubes for use as nerve guidance channels. Biomaterials. 2002; 23:3843–51. [PubMed: 12164188]

[34]. Tsai EC, Dalton PD, Shoichet MS, Tator CH. Synthetic hydrogel guidance channels facilitate regeneration of adult rat brainstem motor axons after complete spinal cord transection. J Neurotrauma. 2004; 21:789–804. [PubMed: 15253805]

[35]. Mukherjee D, Zhao J. The Role of chemokine receptor CXCR4 in breast cancer metastasis. Am J Cancer Res. 2013; 3:46–57. [PubMed: 23359227]

[36]. Muller A, Homey B, Soto H, Ge N, Catron D, Buchanan ME, McClanahan T, Murphy E, Yuan W, Wagner SN, Barrera JL, et al. Involvement of chemokine receptors in breast cancer metastasis. Nature. 2001; 410:50–6. [PubMed: 11242036]

[37]. Yang C, Tibbitt MW, Basta L, Anseth KS. Mechanical memory and dosing influence stem cell fate. Nat Mater. 2014; 13:645–52. [PubMed: 24633344]

[38]. Decher G. Fuzzy nanoassemblies: toward layered polymeric ;ulticomposites. Science. 1997; 277:1232–7.

[39]. Ai H, Jones SA, Lvov YM. Biomedical applications of electrostatic layer-by-layer nano-assembly of polymers, enzymes, and nanoparticles. Cell Biochem Biophys. 2003; 39:23–43. [PubMed: 12835527]

[40]. Thompson MT, Berg MC, Tobias IS, Rubner MF, Van Vliet KJ. Tuning compliance of nanoscale polyelectrolyte multilayers to modulate cell adhesion. Biomaterials. 2005; 26:6836–45. [PubMed: 15972236]

[41]. Schneider A, Francius G, Obeid R, Schwinte P, Hemmerle J, Frisch B, Schaaf P, Voegel JC, Senger B, Picart C. Polyelectrolyte multilayers with a tunable Young's modulus: influence of film stiffness on cell adhesion. Langmuir. 2006; 22:1193–200. [PubMed: 16430283]

[42]. Fourel LVA, Faurobert E, Guillot R, Bourrin-Reynard I, Ren K, Lafanechère L, Planus E, Picart C, Albiges-Rizo C. β3 integrin-mediated spreading induced by matrix-bound BMP-2 controls Smad signaling in a stiffness-independent manner. J Cell Biol. 2016; 212:693–706. [PubMed: 26953352]

[43]. Boudou T, Crouzier T, Ren K, Blin G, Picart C. Multiple functionalities of polyelectrolyte multilayer films: new biomedical applications. Adv Mater. 2010; 22:441–67. [PubMed: 20217734]

[44]. Crouzier T, Ren K, Nicolas C, Roy C, Picart C. Layer-by-layer films as a biomimetic reservoir for rhBMP-2 delivery: controlled differentiation of myoblasts to osteoblasts. Small. 2009; 5:598–608. [PubMed: 19219837]

[45]. Dalonneau F, Liu XQ, Sadir R, Almodovar J, Mertani HC, Bruckert F, Albiges-Rizo C, Weidenhaupt M, Lortat-Jacob H, Picart C. The effect of delivering the chemokine SDF-1alpha in a matrix-bound manner on myogenesis. Biomaterials. 2014; 35:4525–35. [PubMed: 24612919]

[46]. Gribova V, Gauthier-Rouviere C, Albiges-Rizo C, Auzely-Velty R, Picart C. Effect of RGD functionalization and stiffness modulation of polyelectrolyte multilayer films on muscle cell differentiation. Acta Biomater. 2013; 9:6468–80. [PubMed: 23261924]

[47]. Ren K, Crouzier T, Roy C, Picart C. Polyelectrolyte multilayer films of controlled stiffness modulate myoblast cells differentiation. Adv Funct Mater. 2008; 18:1378–89. [PubMed: 18841249]

[48]. Boudou T, Crouzier T, Auzely-Velty R, Glinel K, Picart C. Internal composition versus the mechanical properties of polyelectrolyte multilayer films: the influence of chemical cross-linking. Langmuir. 2009; 25:13809–19. [PubMed: 20560550]

[49]. Laguri C, Sadir R, Rueda P, Baleux F, Gans P, Arenzana-Seisdedos F, Lortat-Jacob H. The novel CXCL12gamma isoform encodes an unstructured cationic domain which regulates bioactivity and interaction with both glycosaminoglycans and CXCR4. PLoS One. 2007; 2:e1110. [PubMed: 17971873]

[50]. Nobes CD, Hall A. Rho, rac, and cdc42 GTPases regulate the assembly of multimolecular focal complexes associated with actin stress fibers, lamellipodia, and filopodia. Cell. 1995; 81:53–62. [PubMed: 7536630]

[51]. So JY, Lee HJ, Kramata P, Minden A, Suh N. Differential Expression of Key Signaling Proteins in MCF10 Cell Lines, a Human Breast Cancer Progression Model. Mol Cell Pharmacol. 2012; 4:31–40. [PubMed: 24558516]

[52]. Meincke M, Tiwari S, Hattermann K, Kalthoff H, Mentlein R. Near-infrared molecular imaging of tumors via chemokine receptors CXCR4 and CXCR7. Clin Exp Metastasis. 2011; 28:713–20. [PubMed: 21735100]

[53]. Salazar N, Munoz D, Kallifatidis G, Singh RK, Jorda M, Lokeshwar BL. The chemokine receptor CXCR7 interacts with EGFR to promote breast cancer cell proliferation. Mol Cancer. 2014; 13:198. [PubMed: 25168820]

[54]. Lechertier T, Berard M, Vassy R, Herve MA, Crepin M. Transendothelial migration of two metastatic breast carcinoma cells depend on the SDF-lalpha-CXCR4 complexes. Anticancer Res. 2004; 24:4011–7. [PubMed: 15739262]

[55]. Nelson MT, Short A, Cole SL, Gross AC, Winter J, Eubank TD, Lannutti JJ. Preferential, enhanced breast cancer cell migration on biomimetic electrospun nanofiber 'cell highways'. BMC Cancer. 2014; 14:825. [PubMed: 25385001]

[56]. Liang Z, Wu T, Lou H, Yu X, Taichman RS, Lau SK, Nie S, Umbreit J, Shim H. Inhibition of breast cancer metastasis by selective synthetic polypeptide against CXCR4. Cancer Res. 2004; 64:4302–8. [PubMed: 15205345]

[57]. Tzircotis G, Thorne RF, Isacke CM. Chemotaxis towards hyaluronan is dependent on CD44 expression and modulated by cell type variation in CD44-hyaluronan binding. J Cell Sci. 2005; 118:5119–28. [PubMed: 16234326]

[58]. Morini M, Mottolese M, Ferrari N, Ghiorzo F, Buglioni S, Mortarini R, Noonan DM, Natali PG, Albini A. The alpha 3 beta 1 integrin is associated with mammary carcinoma cell metastasis, invasion, and gelatinase B (MMP-9) activity. Int J Cancer. 2000; 87:336–42. [PubMed: 10897037]

[59]. Taherian A, Li X, Liu Y, Haas TA. Differences in integrin expression and signaling within human breast cancer cells. BMC Cancer. 2011; 11:293. [PubMed: 21752268]

[60]. Steffen A, Faix J, Resch GP, Linkner J, Wehland J, Small JV, Rottner K, Stradal TE. Filopodia formation in the absence of functional WAVE- and Arp2/3-complexes. Mol Biol Cell. 2006; 17:2581–91. [PubMed: 16597702]

[61]. Mattila PK, Lappalainen P. Filopodia: molecular architecture and cellular functions. Nat Rev Mol Cell Biol. 2008; 9:446–54. [PubMed: 18464790]

[62]. Kayali AG, Van Gunst K, Campbell IL, Stotland A, Kritzik M, Liu G, Flodstrom-Tullberg M, Zhang YQ, Sarvetnick N. The stromal cell-derived factor-1alpha/CXCR4 ligand-receptor axis is critical for progenitor survival and migration in the pancreas. J Cell Biol. 2003; 163:859–69. [PubMed: 14638861]

[63]. Peng SB, Peek V, Zhai Y, Paul DC, Lou Q, Xia X, Eessalu T, Kohn W, Tang S. Akt activation, but not extracellular signal-regulated kinase activation, is required for SDF-1alpha/CXCR4-mediated migration of epitheloid carcinoma cells. Mol Cancer Res. 2005; 3:227–36. [PubMed: 15831676]

[64]. Vlahakis SR, Villasis-Keever A, Gomez T, Vanegas M, Vlahakis N, Paya CV. G protein-coupled chemokine receptors induce both survival and apoptotic signaling pathways. J Immunol. 2002; 169:5546–54. [PubMed: 12421931]

[65]. Nervi B, Link DC, DiPersio JF. Cytokines and hematopoietic stem cell mobilization. J Cell Biochem. 2006; 99:690–705. [PubMed: 16888804]

[66]. Dorsam RT, Gutkind JS. G-protein-coupled receptors and cancer. Nat Rev Cancer. 2007; 7:79–94. [PubMed: 17251915]

[67]. Domanska UM, Kruizinga RC, Nagengast WB, Timmer-Bosscha H, Huls G, de Vries EG, Walenkamp AM. A review on CXCR4/CXCL12 axis in oncology: no place to hide. Eur J Cancer. 2013; 49:219–30. [PubMed: 22683307]

[68]. Xu TP, Shen H, Liu LX, Shu YQ. The impact of chemokine receptor CXCR4 on breast cancer prognosis: a meta-analysis. Cancer Epidemiol. 2013; 37:725–31. [PubMed: 23763828]

[69]. Zhang Z, Ni C, Chen W, Wu P, Wang Z, Yin J, Huang J, Qiu F. Expression of CXCR4 and breast cancer prognosis: a systematic review and meta-analysis. BMC Cancer. 2014; 14:49. [PubMed: 24475985]

[70]. Kang H, Mansel RE, Jiang WG. Genetic manipulation of stromal cell-derived factor-1 attests the pivotal role of the autocrine SDF-1-CXCR4 pathway in the aggressiveness of breast cancer cells. Int J Oncol. 2005; 26:1429–34. [PubMed: 15809737]

[71]. Migliorini E, Thakar D, Sadir R, Pleiner T, Baleux F, Lortat-Jacob H, Coche-Guerente L, Richter RP. Well-defined biomimetic surfaces to characterize glycosaminoglycan-mediated interactions on the molecular, supramolecular and cellular levels. Biomaterials. 2014; 35:8903–15. [PubMed: 25088726]

[72]. Avigdor A, Goichberg P, Shivtiel S, Dar A, Peled A, Samira S, Kollet O, Hershkoviz R, Alon R, Hardan I, Ben-Hur H, et al. CD44 and hyaluronic acid cooperate with SDF-1 in the trafficking of human CD34+ stem/progenitor cells to bone marrow. Blood. 2004; 103:2981–9. [PubMed: 15070674]

[73]. Crouzier T, Fourel L, Boudou T, Albiges-Rizo C, Picart C. Presentation of BMP-2 from a soft biopolymeric film unveils its activity on cell adhesion and migration. Adv Mater. 2011; 23:H111–8. [PubMed: 21433098]

[74]. Hesselgesser J, Liang M, Hoxie J, Greenberg M, Brass LF, Orsini MJ, Taub D, Horuk R. Identification and characterization of the CXCR4 chemokine receptor in human T cell lines: ligand binding, biological activity, and HIV-1 infectivity. J Immunol. 1998; 160:877–83. [PubMed: 9551924]

[75]. Schwartz MA, Schaller MD, Ginsberg MH. Integrins: emerging paradigms of signal transduction. Annu Rev Cell Dev Biol. 1995; 11:549–99. [PubMed: 8689569]

[76]. Yamada KM, Miyamoto S. Integrin transmembrane signaling and cytoskeletal control. Curr Opin Cell Biol. 1995; 7:681–9. [PubMed: 8573343]

[77]. Miranti CK, Brugge JS. Sensing the environment: a historical perspective on integrin signal transduction. Nat Cell Biol. 2002; 4:E83–90. [PubMed: 11944041]

[78]. Levental KR, Yu H, Kass L, Lakins JN, Egeblad M, Erler JT, Fong SF, Csiszar K, Giaccia A, Weninger W, Yamauchi M, et al. Matrix crosslinking forces tumor progression by enhancing integrin signaling. Cell. 2009; 139:891–906. [PubMed: 19931152]

[79]. Chen L, Bourguignon LY. Hyaluronan-CD44 interaction promotes c-Jun signaling and miRNA21 expression leading to Bcl-2 expression and chemoresistance in breast cancer cells. Mol Cancer. 2014; 13:52. [PubMed: 24606718]

[80]. Louderbough JM, Schroeder JA. Understanding the dual nature of CD44 in breast cancer progression. Mol Cancer Res. 2011; 9:1573–86. [PubMed: 21970856]

[81]. Shipitsin M, Campbell LL, Argani P, Weremowicz S, Bloushtain-Qimron N, Yao J, Nikolskaya T, Serebryiskaya T, Beroukhim R, Hu M, Halushka MK, et al. Molecular definition of breast tumor heterogeneity. Cancer Cell. 2007; 11:259–73. [PubMed: 17349583]

[82]. Zhou L, Guo X, Jing BA, Zhao L. CD44 is involved in CXCL-12 induced acute myeloid leukemia HL-60 cell polarity. Biocell. 2010; 34:91–4. [PubMed: 20925198]

[83]. Fuchs K, Hippe A, Schmaus A, Homey B, Sleeman JP, Orian-Rousseau V. Opposing effects of high- and low-molecular weight hyaluronan on CXCL12-induced CXCR4 signaling depend on CD44. Cell Death Dis. 2013; 4:e819. [PubMed: 24091662]

[84]. Alsayed Y, Ngo H, Runnels J, Leleu X, Singha UK, Pitsillides CM, Spencer JA, Kimlinger T, Ghobrial JM, Jia X, Lu G, et al. Mechanisms of regulation of CXCR4/SDF-1 (CXCL12)-dependent migration and homing in multiple myeloma. Blood. 2007; 109:2708–17. [PubMed: 17119115]

[85]. Murphy LO, Blenis J. MAPK signal specificity: the right place at the right time. Trends Biochem Sci. 2006; 31:268–75. [PubMed: 16603362]

[86]. Sharrocks AD. Cell cycle: sustained ERK signalling represses the inhibitors. Current biology : CB. 2006; 16:R540–2. [PubMed: 16860730]

[87]. Bid HK, Roberts RD, Manchanda PK, Houghton PJ. RAC1: an emerging therapeutic option for targeting cancer angiogenesis and metastasis. Mol Cancer Ther. 2013; 12:1925–34. [PubMed: 24072884]

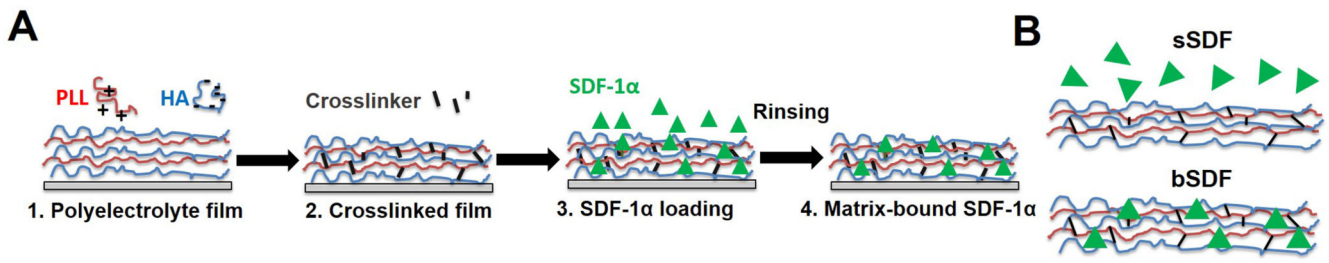

Figure 1.

(A) Successive steps for the preparation of matrix-bound SDF-1α using layer-by-layer films as ECM matrix with poly(L-lysine) (PLL) and hyaluronan (HA) as polyelectrolytes. The film is first deposited step-by-step (1), then cross-linked (2) and finally loaded with SDF-1α in acidic conditions (1 mM HCl) (3), followed by a rinsing step in order to obtain matrix-bound SDF-1α (4). (B) SDF-1α can be presented as a soluble cue (sSDF) or in a matrix-bound manner (bSDF).

Europe PMC Funders Author Manuscripts

Europe PMC Funders Author Manuscripts

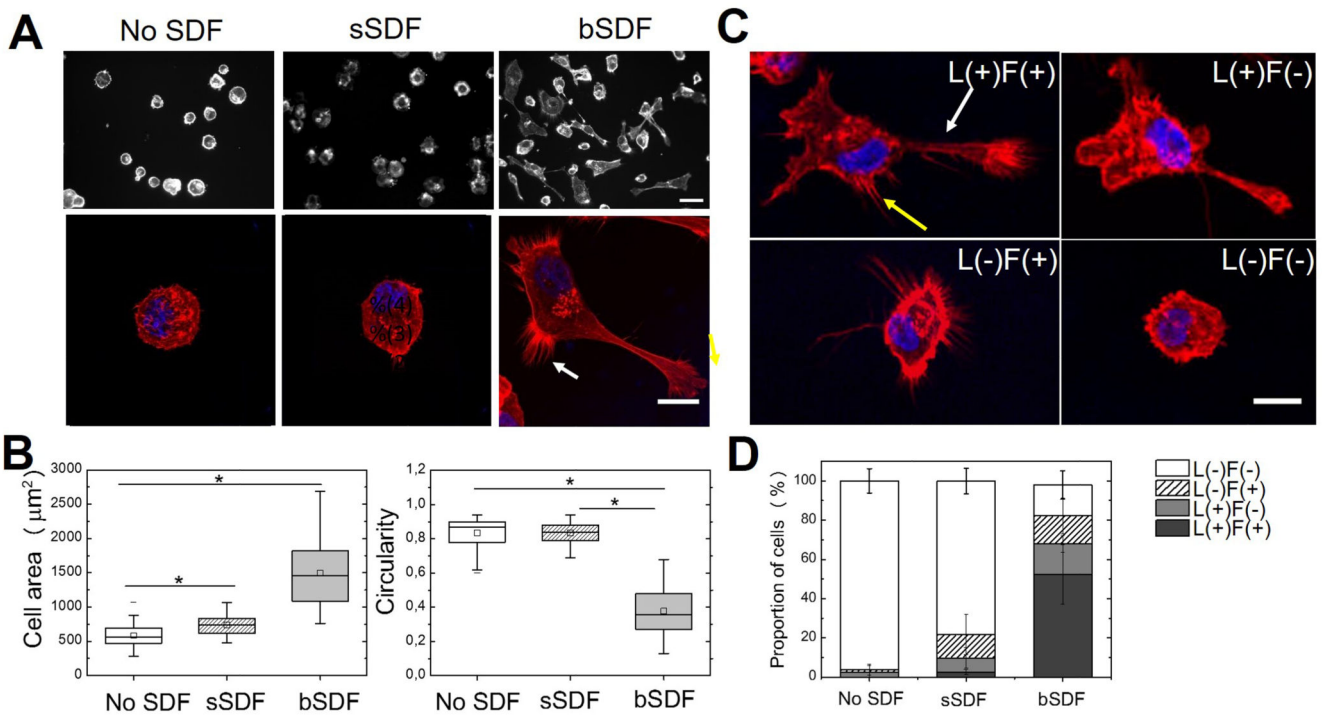

Figure 2.

Effect of matrix-bound SDF-1α on cell spreading and protrusion formation. Cell morphology was observed 16 h after plating by staining the actin cytoskeleton with rhodamine phalloidin (red) and the nuclei with DAPI (blue). MDA-MB-231 cells were grown on films with No SDF, sSDF, and bSDF: (A) Upper row: fluorescence images, scale bar: 50 μm; lower row: confocal fluorescence images, scale bar: 20 μm,; the yellow arrow indicates lamellipodia and the white arrow indicates filopodia. (A') Quantitative analysis of the cell spreading area and circularity. At least 50 cells were analyzed for each experimental condition in each independent experiment. Experiments were performed at least in duplicate (ie at least two independent experiments). * $p < 0.05$ in comparison to control (Anova one way on ranks). (B) Representative images of MDA-MB-231 cells exhibiting four major phenotypes depending on their protrusions, whether they had Lamellipodia (L+ or L-) and/or Filopodia (F+ or F-) : L+/F+, L+/F-; L-/F+ and L-/F-. Scale bar: 20 μm; (B') Quantitative analysis of the % of each L/F phenotype in the presence of sSDF and bSDF in comparison to the absence of SDF (No SDF). At least 50 cells were analyzed for each experimental condition. Experiments were performed in duplicate.

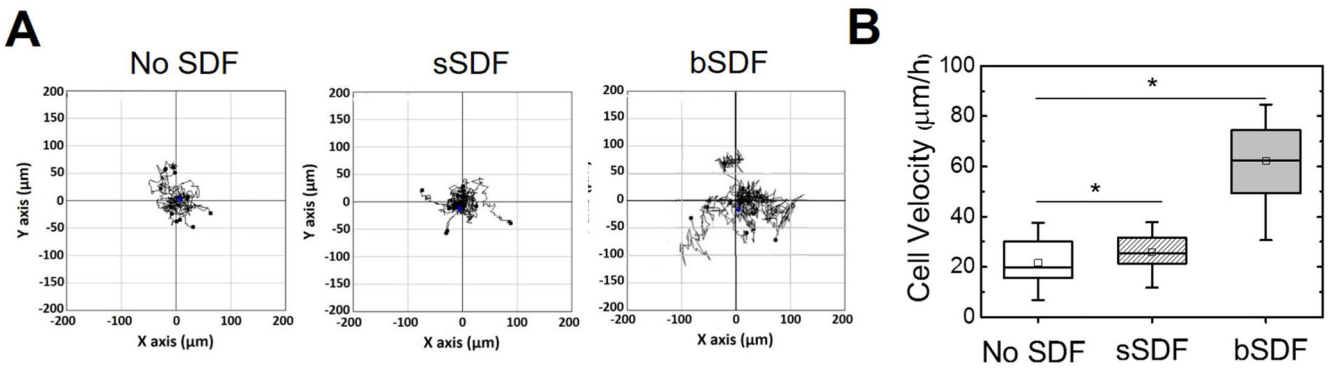

Figure 3.

bSDF potentiates breast cancer cell migration. (A) Representative trajectories of MDA-MB-231 cells on polyelectrolyte films for the three experimental groups (No SDF, sSDF and bSDF). (B) Quantitative analysis of the cell migration speeds. At least 20 cells were analyzed for each experimental condition. Experiments were performed at least in duplicate. $*p < 0.05$.

Europe PMC Funders Author Manuscripts

Europe PMC Funders Author Manuscripts

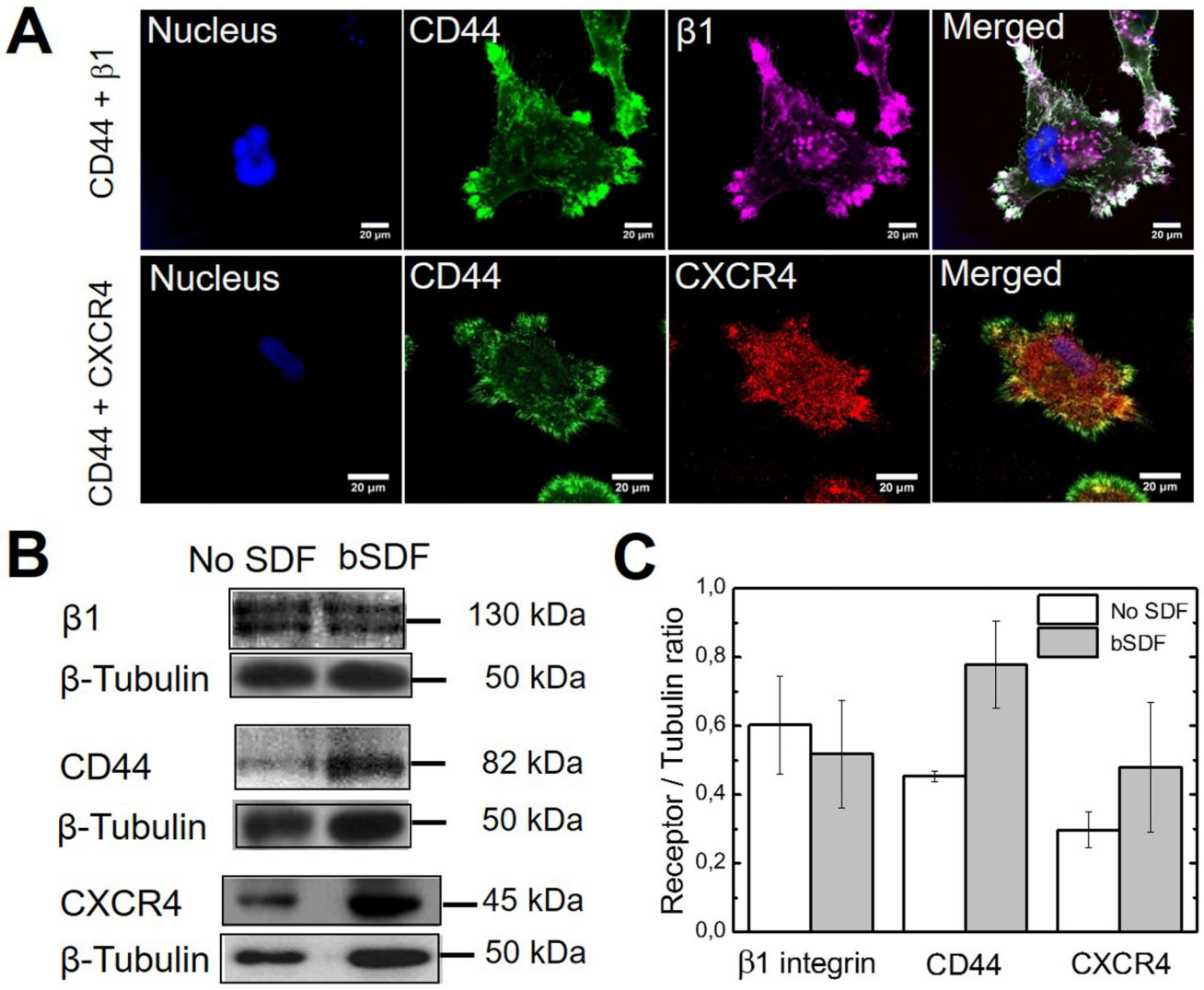

Figure 4.

SDF-1α receptor and cell adhesion receptors staining and expression in response to bSDF. (A) MDA-MB-231 cells were seeded onto the films with bSDF for 16 h. Staining of CD44 (green), CXCR4 (red), β1 integrin (purple) and nuclei (blue) are shown; scale bar: 20 μm; (B) Western blot analysis of CD44, CXCR4 and β1 integrin expression reveals a change in the expression of CD44 and to a lesser extent CXCR4 for bSDF in comparison to the absence of SDF (No SDF). Tubulin was used as a control. The molecular weight of each band is indicated. (C) Quantification of the band intensity from the Western blots for each receptor. The ratio of the receptor/tubulin bands were calculated (n = 3 independent experiments, data are mean ± SD).

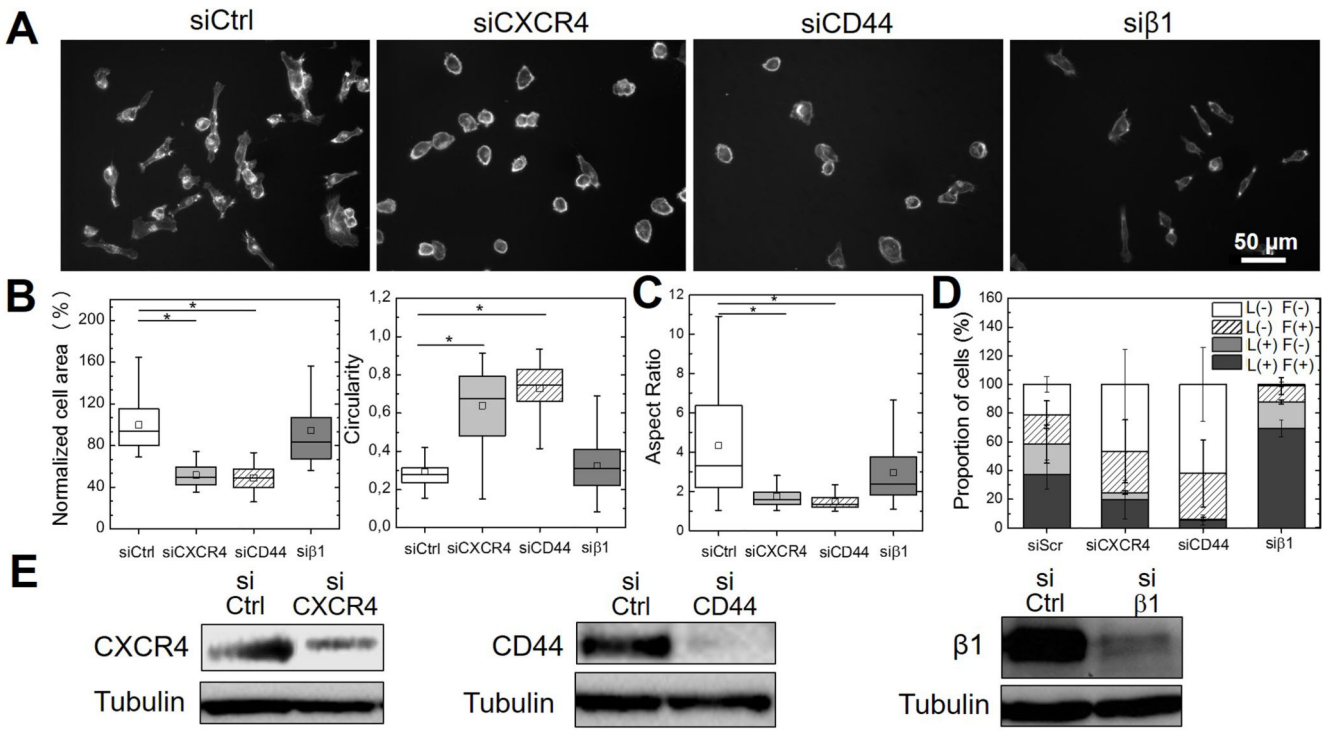

Figure 5.

Effects of CXCR4, CD44 and β1 integrin silencing on bSDF-induced cell spreading and protrusion formation. CD44, CXCR4 and β1 integrin were knocked-down in MDA-MA-232 cells using specific siRNAs before cells were seeded onto bSDF films for 16 h. (A) Representative images of cancer cells after receptor silencing of CXCR4, CD44 and β1 integrin in comparison to control siRNA; (B) Quantitative analysis of the cell spreading area, circularity and (C) aspect ratio. (D) The quantitative analysis of the distribution of the four protrusion phenotypes is also given. For the quantifications, at least 50 cells were analyzed for each experimental condition in each independent experiment. * $p < 0.05$ in comparison to control (Anova one way on ranks). Three independent experiments were performed. (E) Western Blot showing the effective decrease of receptor expression (CXCR4, CD44, β1 integrin) after siRNA-mediated silencing. Cells were transfected with a scrambled siRNA as a control.

Europe PMC Funders Author Manuscripts

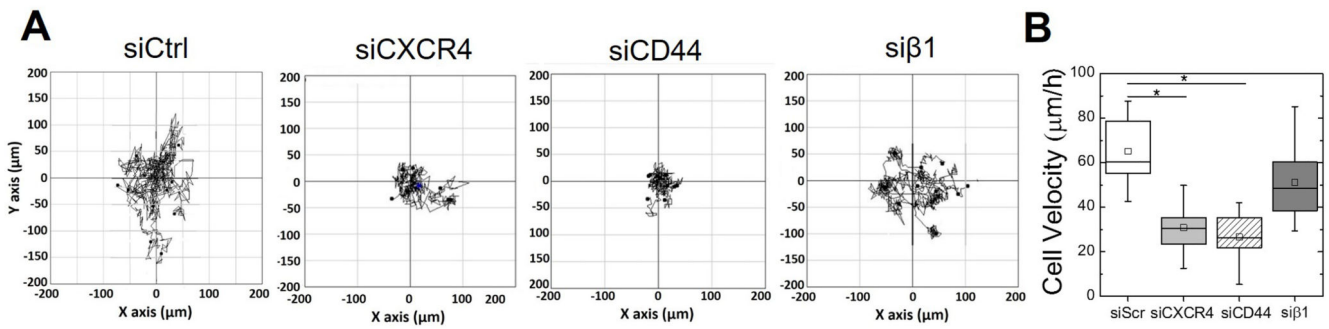

Figure 6.

Effects of CXCR4, CD44 and β1 integrin silencing on bSDF-induced cell migration. CD44, CXCR4 and β1 integrin were knocked-down using specific siRNA before cells were seeded onto bSDF films for 16 h (same conditions as for Figure 5) (A) Representative trajectories of MDA-MB-231 cells on bSDF films after silencing of the different receptors. (B) Quantitative analysis of the cell migration speed. At least 20 cells were analyzed for each experimental condition in each experiment. Two independent experiments were performed. * $p < 0.05$ in comparison to control ((Anova one way on ranks).

Europe PMC Funders Author Manuscripts

Europe PMC Funders Author Manuscripts

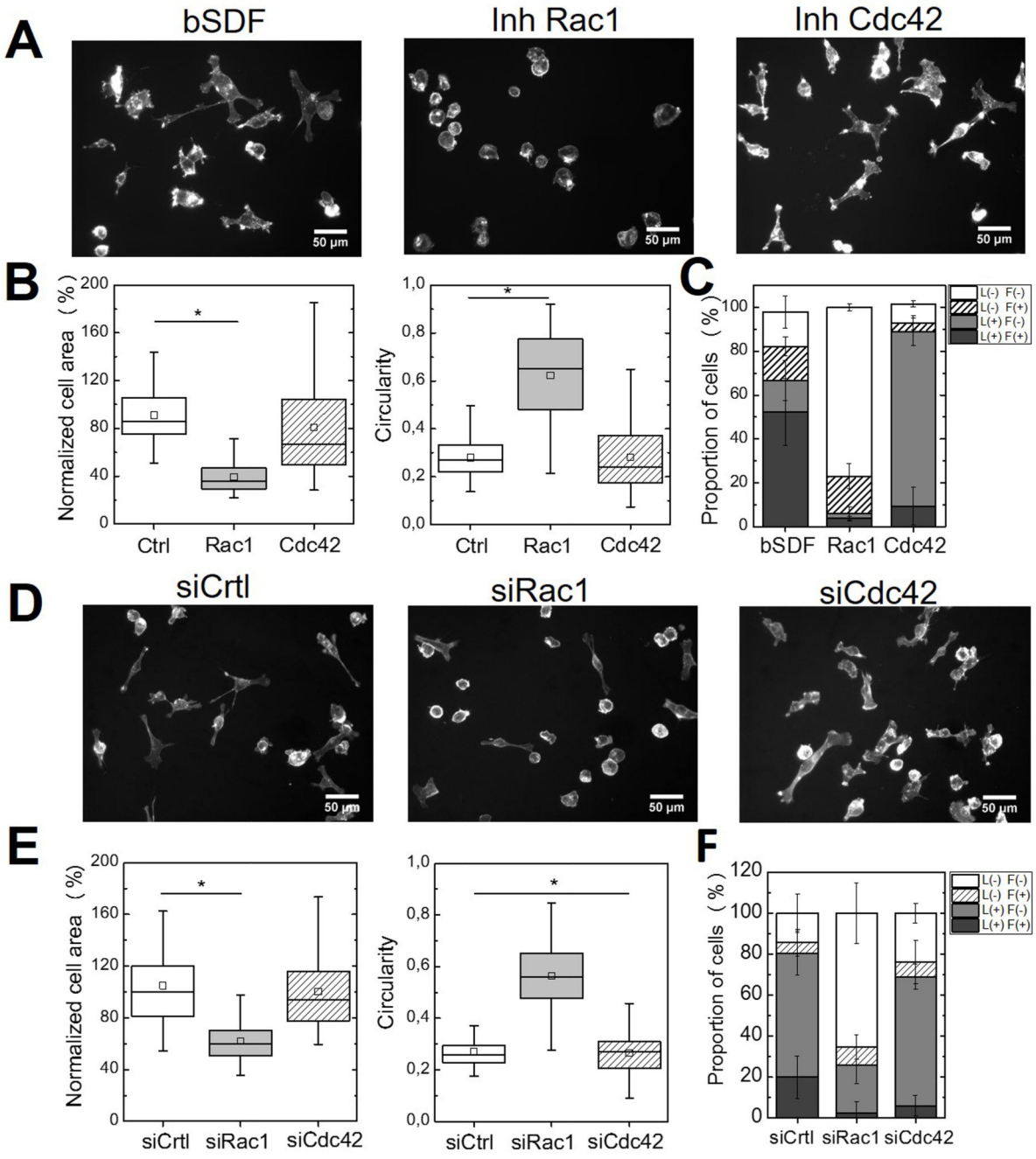

Figure 7.

Effects of drug inhibition or of siRNA-medicated silencing of Rac1 and Cdc42 on bSDF-induced cell spreading and protrusion formation. These effects were assessed 16 h after cell seeding. (A) Fluorescence images (actin staining) of MDA-MB-231 cells seeded onto bSDF films in the presence of Rac1 inhibitor (NSC23766) or Cdc42 inhibitor (ML141). (B) Quantitative analysis of the cell spreading area, circularity and (C) proportion of cells in each depending on their protrusion phenotypes. (D) Representative fluorescence images of cells after silencing using siRNA against Rac1 and Cdc42 and (E) corresponding

quantitative analysis (same parameters as in F). At least 50 cells were analyzed for each experimental condition for each experiment. Two independent experiments were performed. *$p < 0.05$ (Anova one way on ranks).

Europe PMC Funders Author Manuscripts

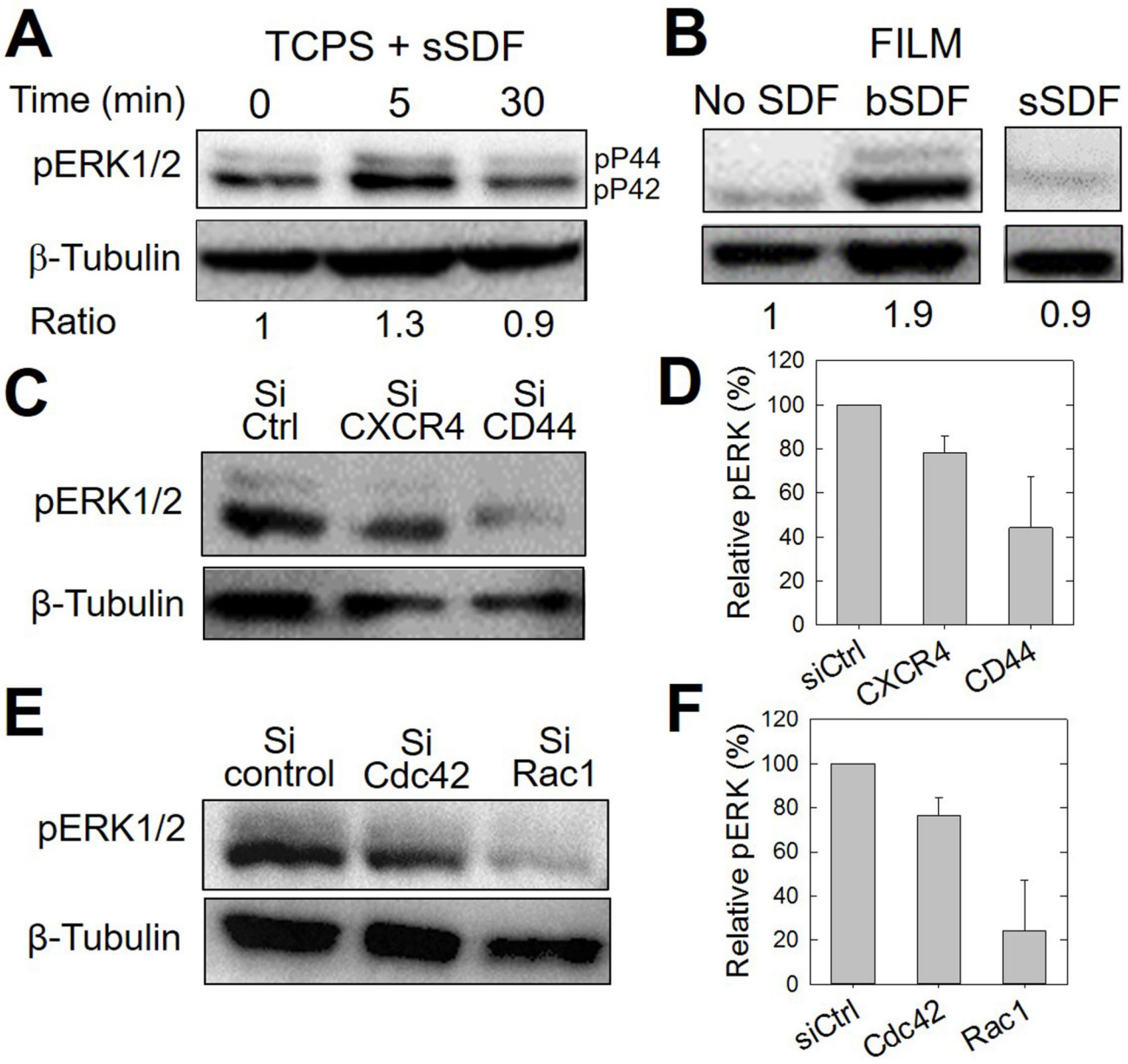

Figure 8.

CD44 involvement in CXCR4-medicated and bSDF-induced ERK1/2 phosphorylation in MDA-MB231 breast cancer cells. The different panels show representative western blots and their corresponding quantitative analysis using anti-phosphoERK1/2 antibodies (pERK) to reveal changes in the phosphorylation of ERK1/2. (A) Serum-starved MDA-MB-231 cells cultured on tissue culture polystyrene (TCPS) were used as a control to assess early ERK phosphorylation. The basal level was quantified after 5 min and 30 min of stimulation in a serum-containing medium. β-tubulin was taken as a control. The band intensity ratios (pERK1/2 / tubulin) are also given, the Time 0 being considered as a reference (arbitrarily set to 1). (B) pERK activation of cancer cells, cultured for 16 h on polyelectrolyte films in the absence (No SDF), with SDF-1α presented at the ventral side of the cells (bSDF), or

Europe PMC Funders Author Manuscripts

with SDF-1α added in the growth medium (sSDF). The band intensity ratios are also given, the condition “No SDF” being set arbitrarily to 1. (C) pERK activation after selective CXCR4 and CD44 knock-down using siRNAs and (D) corresponding quantification of pERK/tubulin ratios, the control silencing being arbitrarily set to 100%. Two independent experiments were performed. (Data are mean ± SD). (E) pERK activation after selective Cdc42 and Rac1 knock-down using siRNAs and (F) corresponding quantification of pERK/tubulin ratios, the control silencing being arbitrarily set to 100%. Two independent experiments were performed. (Data are mean ± SD).

Europe PMC Funders Author Manuscripts

Europe PMC Funders Author Manuscripts

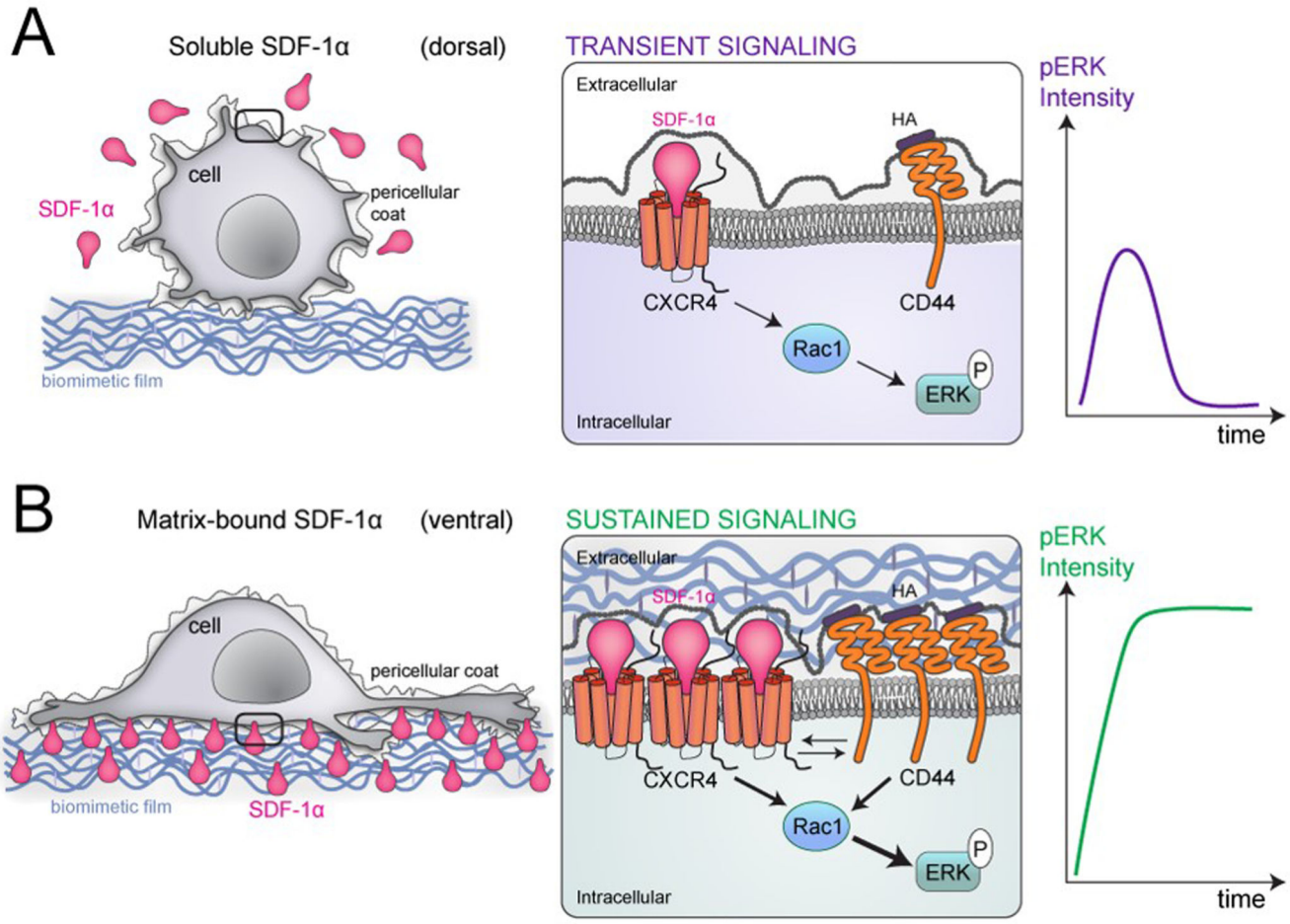

Figure 9.

Scheme summarizing the major differences in the response of MDA-MB-231 cancer cells to SDF-1α presented either as soluble cue (A) or as matrix-bound cue (B) for MDA-MB-231 breast cancer cells at different length scales from left to right. Left: at the cellular scale; middle at the plasma membrane/receptor scale and right: consequence in terms of phospho-ERK signaling. In the case of a soluble presentation (sSDF) (A), the local concentration of SDF-1α molecules is very low and SDF-1α is mostly presented at the dorsal side of the cells. As a consequence, cell adhesion is low and cells are round with only few protrusions. In this case, the signaling is transient since the CXCR4 and hyaluronan receptors (CD44 being the major one in MDA-MB231 cells) are only scarce and do not cooperate. SDF-1α-induced signaling via CXCR4 activates Rac1 and pERK but the intensity of the signal is small and its duration is transient (right scheme). In the case of matrix-bound SDF-1α (bSDF), the local concentration of SDF-1α in the polyelectrolyte film is locally very high so the cellular receptors (CXCR4), which are mostly localized at the basal side of the cancer cells, can bind to their SDF-1α ligands. This induces a localized receptor clustering (middle scheme) for CXCR4 as well as for the HA receptor. Indeed hyaluronan, the CD44 ligand, is provided by the pericellullar coat of cancer cells and by the polyelectrolyte film, which is made of HA. In this situation of spatial confinement at the ventral side of the cell, the two

receptors CXCR4 (for SDF-1α) and CD44 (for HA) act in concert and activate Rac1 and the subsequent phosphorylation of ERK1/2. As a consequence, the intensity of the pERK signal is very high and it is sustained over a long time, for at least 16 h as shown in Figure 8B.

Europe PMC Funders Author Manuscripts